Chapter 14
Plasmon Assisted Luminescence in Rare Earth Doped Glasses

M. Reza Dousti and Raja J. Amjad

Abstract Incorporation of metallic nanoparticles in rare earth doped oxide glasses has been introduced as an interesting method to enhance their optical properties. Controlling the size and shape of metallic nanoparticles is a challenging issue which depends strongly and ambiguously on concentration, time and temperature of heat-treatments. In this chapter, we firstly revisit the importance of materials science in general and the rare-earth doped glasses in particular. The performance of rare earth ions in glassy matrices, the probable interactions and the related theories are discussed. Moreover, the incorporation of metallic nanoparticles and their effect on modification of optical properties of rare earth doped glasses is reviewed. Finally, several examples of enhancement and quenching of stokes and anti-stokes luminescence of rare earth ions doped in different glasses are summarized. The incorporation of the metallic nanoparticles is a promising method to improve the optical properties of different oxide glasses for diverse applications such as amplifiers, solid state lasers, sensors, etc. However, to understand the complete role of metallic nanoparticles and control their size distribution and shape, further research is necessary.

Keywords Rare earth doped glasses • Metallic nanoparticles • Amorphous nanocomposites • Optical materials

The necessity to develop noble materials for various applications – from decorative objects, optoelectronic devices, and military facilities, to medical interferences such as drug-deliverers, artificial bones and sturdy dental ceramics – has motivated the materials engineers and scientists to demand for new materials, with low-cost, high efficiency, long durability and recyclability. Glass and glass-ceramic technology is classified to be among the most important branch in the materials science since these composites could provide a wide range of optical, chemical, thermal,

M.R. Dousti (✉)
Instituto de Física de São Carlos, Universidade de São Paulo, 13560-970 São Carlos, SP, Brazil
e-mail: mrdousti@ifsc.usp.br; mrdphysics@gmail.com

R.J. Amjad
Department of Physics, COMSATS Institute of Information Technology, Lahore 54000, Pakistan
e-mail: rajajunaid25@gmail.com; mjunaidamjad@ciitlahore.edu.pk

C.D. Geddes (ed.), *Reviews in Plasmonics 2015*,
DOI 10.1007/978-3-319-24606-2_14

electrical and magnetic properties due to the large diversity in their structure and compositional elements. Glasses, by definition, are non-crystalline solids which show glass transition temperature and can form the glass-ceramics by the controlled heat-treating procedures. Glasses have emerged in various fields and show significant contribution in development of new functional materials. Glass-ceramics show typically better mechanical, thermal and optical performance than their mother counterpart, due to the partial presence of nano- or micro-crystalline structures. The glasses and glass ceramics can be used as solders, laser hosts, memory planes, switching panels, optical fibers, sensors, lenses, optical limiters, waveguides, army devices, medical devices and dental materials etc. The research on the glassy materials shows a rapid growth as evaluated by a recent analysis of the major scientific databases. The glasses are widely used as optical materials as they usually show a wide transparency in the ultraviolet (UV) to near-infrared (NIR) region and non-linear optical absorption, which could be combined with their other promising properties to obtain novel materials. When doped with rare earth (RE) ions, the glasses can emit in a wide range of spectral energy; from ultraviolet to visible and to near-infrared and far-infrared regions. The intensity, peak wavelength, excited state lifetime and quantum efficiency of those emissions are determinant characteristics of the RE-doped materials which could be engineered by selection of the host glass, concentration of RE ions, the co-doping species, heat-treatments etc. For example, the selection of the glass hosts with low phonon energies, can reduce the nonradiative losses, and increases the quantum efficiency, while upconversion emissions could occur to generate a high energy photon, through the excitation of the RE ions by two incoming photons. The upconversion (anti-Stokes) and normal (Stokes) emissions in the RE-doped glasses are mainly favored by the various energy transfer mechanisms among the neighboring ions. Such energy transfer processes are listed in this review paper and discussed in details. Moreover, the Judd-Ofelt formalism as the most important theoretical approach to evaluate the radiative properties of RE ions is also revisited. The radiative properties such as emission cross-section of most of the RE ions in the current glasses is not very effective to obtain a high quantum yield device, and in most of the cases, increasing the concentration of RE ions results in the concentration quenching effect. Therefore, improving the emission efficiency of the RE ions is the current issue and several proposals have been demonstrated to optimize the latter properties. For example, the incorporation of Yb^{3+} ions or metallic species as the sensitizers, or addition of shells or OH-removers which could decrease the quenching centers.

On the other hand, the incorporation of metallic particles (such as nanoparticles, clusters, atoms, dimers, ions, etc) has attracted a large interest due to the remarkable interaction of the excitation beam with the electronic structure of the metal. Meanwhile, in the last decade, nanoscience and nanotechnology has been merged as a new filed of science which attempt to synthesize the particles having dimensions in the order of few nanometers to a hundred of nanometers and to embed and confine such particles in several functional materials. In the nanosized metallic particle, the interaction of the light with metal results in the so-called surface plasmon resonance which is the collective oscillations of the electrons of the

metal, thereby, it modifies the optical, electrical and structural properties of the containing host, especially the dielectric glassy media which will be discussed in this work. The glass containing metallic nanoparticles has gained a large interest thanks to their potentiality to develop waveguides, optical limiters, micro-lenses, non-linear devices, solid state batteries, electrochemical sensors etc. On the other hand, it has been also proposed that the optical properties (emission intensity) of the RE doped glasses could be altered by embedding the metallic nanoparticles. The latter application is the main aim of this chapter. Beside a great number of reports on the enhancement and quenching of the emissions of the RE ions doped glasses by incorporation of metallic species, the origins of both enhanced or quenched luminescence is still not fully understood and needs further attention. Several works have shown that the metallic nanoparticles could improve the emission intensity of RE ions (e.g. Eu^{3+}, Er^{3+}, Nd^{3+}, Tb^{3+} etc) doped glasses. The size of particles observed in those reports could vary from a few angstrom to tens of nanometer, while in many cases the plasmon resonance absorption band are not observed. On the other hand, the quenching in the luminescence of some RE ions (mainly Dy^{3+}, and Sm^{3+} etc) has been observed in presence of metallic nanoparticles, while there are several reports which attributed the enhancement of the luminescence to other metallic species such as ions, dimers, clusters, etc, rather than the nanoparticles. However, up to this stage, the contribution of each species in luminescence intensification is not clearly understand. Therefore, in this work, we would like to review the existing literature, up to our knowledge and time, on the history of the glass science and technology, the optical properties of rare earth doped glasses and their relevant theories, which would be followed by an introduction on the importance of the nanoscience with an emphasizing on the optical properties of the nanoparticles in an dielectric media. We will also discuss the important characteristics of the metallic nanoparticles, such as size and shape of them, which could alter their optical properties. The Mie theory, and related theories to understand the optical properties of nanoparticles, their formation and growth mechanisms are also discussed in this review paper. Later, the most utilized spectroscopic and imaging techniques to characterize the nanoparticles will be quickly overviewed. At the end, the effect of metallic species (mainly nanoparticles) on the absorption and luminescence characteristics of the RE doped glasses will be discussed according to the existing literature.

14.1 Glasses and Glass Ceramics

Nowadays, materials science is a crucial area of research due to the limited range of organic materials on earth to supply fuels and power for living, factories and technology. Therefore, lot of efforts have been put on the design of new materials to alternate inorganic sources. Solar cells are good example of those substances. Polymers, ceramics, glasses and new light sources based on lasers, amplifiers in networking, Li-ion batteries, etc are some of the new materials which emerged to

assist the "green energy" agenda. Currently, glasses exist all around the world and on our daily life, starting from drinking cups to the dressing mirrors, from electric lamps to the communication fibers, from window glass to wine bottle and many attractive decorative jams. There are magnificent collections and museum of glasses which inspire the human mind by those timeless and limitless colorful and shaped objects of art. The first glass on the earth, indeed, has been made by nature. The ashes of overflowed volcanoes get cooled down slowly and made natural glasses, containing aluminum silicon, sodium, potassium, calcium and iron.

But, what is a glass? Glass is an amorphous solid (non-crystalline) material which has no long- or short-range order. It shows a glass transition, which is the reversible transition from a rigid and relatively brittle state into a molten or rubber-like state. Glasses are usually fragile and preferably transparent in visible region. Glasses can be formed by cooling a melt rapidly to glass transition temperature such that the quenching time is insufficient to form any crystalline phase. In discipline, the glass is referred to all non-crystalline solids (with an amorphous structure), exhibiting a glass transition when heated towards the liquid state. Therefore, glasses can be classified to various sorts of materials, such as ionic melts, metallic alloys, aqueous solutions, molecular liquids, and polymers.

On the other hand, glasses can be transformed to glass-ceramics (polycrystalline materials) by controlled crystallization process. Glass-ceramics possess versatile properties of both glasses and ceramics. The structure of a glass-ceramic includes an amorphous phase and one or more crystalline phases (usually between 30 % and 90 % of whole bulk). Glass-ceramics are among interesting materials since they can be fabricated as easy as glasses, while having advantageous properties of ceramics, such as low porosity, high toughness, strength, low or even negative thermal expansion, high temperature stability, good chemical durability, resorbability, ion conductivity, superconductivity, isolation capabilities, low dielectric constant and loss, better optical and emission properties when doped with rare earth ions, high resistivity and break down voltage. These properties can be engineered by appropriate base glass composition and controlled heat treatment/crystallization process. Glass-ceramics are usually obtained in two steps: Firstly, a glass is formed by the melt-quenching or sol-gel techniques. Then, it is cooled down and is again reheated at an appropriate temperature for a certain time. As a consequence, the glass partly crystallizes. In most cases nucleating agents are added to the base composition of the glass-ceramic. These nucleation agents can speed-up and control the crystallization process. Unlike sintered ceramics, glass-ceramics have no pores, because of no pressing and sintering procedures. They can be mass-produced and their nanostructure can be designed to combine a variety of properties [1].

The history of glasses made by man has started since 4000 B.C. in Mesopotamia, western Asia. These glasses were glazed due to application of copper compounds. Colorful glasses have been prepared between fourteen and sixteen century B.C. in Egypt. However, the art of glass transferred to Syria, Cyprus and Palestine at eleventh century B.C. All nations have used same technique to prepare the glasses; the glasses were melted, drown out and winded around a clay core which was kept by an iron rod. Around 4000 B.C., Greek and Macedonia become centers of glass

makers. They used new approaches such as sandwiching techniques, adding gold layers and colorful mosaics. At third and second century B.C., Roman Empire was emerged which also continued glass blowing up to a new revolution which occurred in Greek Empire and Muslims countries, especially in Syria and Palestine at seventh century A.D. On the other side of the earth, China (second century B.C.) and India (fifth century B.C.) also were heading in blowing the glasses containing barium and lead. In the ninth century, Baghdad was on the headline of art of glass blowing. Persia also became famous in preparing the glasses and grinding the glassy surfaces. In the thirteenth century, once again, Syria became the center of glasses due to conquest of Persia by Chengis Khan, and fantasy mosque lamps in Damascus were built up. However, the war of Timur in Damascus contributed to immigration of many glass makers from Syria to Samarkand. In this time, large tax reliefs and social recognition from European governments pushed the glass makers to develop the techniques of glass blowing. Addition of calcia to make shinier and brilliant glasses (Crystallo-glasses) and "ice glasses" methods were two biggest achievements of that time. After immigration of glass workers from Italy, Germany became a center of glass blowing. Patronage of Church helped the regime to prepare new glasses such as "waldglas" and "potash-lime". In the nineteenth century, Europe, United States, Bohemia and many other countries developed the techniques of glass blowing. In that time, crystals became very popular. Next, fluorescent glasses, Opaline, HF-etched glasses and cobalt blue glasses were prepared [2].

In the twentieth century, by developments of chemistry and physics of inorganic materials, glasses were also grown, not only for decorative objects, and daily life facilities, but for scientific purposes. Silica glass is the first production of this century which was mixed with other oxides such as CaO, PbO and CoO. By understanding the amorphous nature of glasses, study of the local structure and bonding in glasses were acknowledged as important factors. On the other hand, glass blowing became industrialized where the sheets of few millimeters in thickness, couple of meters in width with desirable length were seen using developed machines. The cutting, polishing and coating methods led to develop glass pieces potential for microscope, telescope, glass-fibers (cables), electronic bulbs and beverage bottles [2]. Nuclear wastes are also cleared using borosilicate glasses and calcium phosphate and silicate were emerged in repairing the bones and bio-techniques [3, 4].

More recently, zinc phosphate and lead borate glasses were used as solders [5–7]. Phosphate and fluro-phosphate glasses were applied as laser hosts [8]. Memory panels and switching materials, which turn from resistive to conductors at a certain voltage, were prepared by chalcogenide glasses [9]. Superior transparency of halide glasses made them, recently, a good candidate to be substituted for silica fibers in telecommunication technology [10, 11]. Modern glasses are versatile, from soda-lime silicate, borosilicate and alumina-silicate to borofluorite, phosphate, germanate, antimony and tellurite glasses. They show different physical and optical properties due to their specific structures which make them excellent candidates for applications in different branches of science and technology. In a scientific approach, tellurite glasses attracted large interest due to its significant

optical, thermal and physical properties [12]. Moreover, oxyfluoride glasses have attracted a large attention for optical properties because they provide comparatively low phonon energies and high chemical and mechanical stabilities [13].

Providing diverse applications from solar cells, optical amplifiers, solid state lasers, army tools, and medical devices, the necessity of research on glasses is increased to understand their structure, optophysical properties and functionality. An exponential increase in number of publications in the field of glasses in general and tellurite glass (as an example) in particular is an evident of such needs. Figure 14.1 presents the number of publication on "glasses" and "tellurite glasses" indexed by SCOPUS database from 1930 up to the end of June 2014 [14]. The increased number of publications on the glass technology was also highlighted by Mauro and Zanotto [15]. Analyzing the data given by SCOPUS, they concluded that the China and United States are the frontiers in glasses in terms of number of publications, while Journal of Non-Crystalline Solids is the most significant journal which publishes "glass-related" papers.

Glasses are excellent candidates to host the so called rare earth ions (lanthanides), since they possess large refractive index, wide transparency window, high RE solubility, etc. Rare earth ions show exceptional optical properties such as long lifetimes, sharp absorption intensities, and excellent coherence properties due to their $4f^N$ to $4f^N$ optical transitions and other significant properties like large oscillator strengths, broad absorption and emission bands and short lifetimes due to their $4f^N$ to $4f^{N-1}5d$ transitions [16]. Special optical properties of the RE ions and their photonic applications in addition to nonradiative (NR) energy transfer (ET) processes led to a wide study on REs. In principle, ET processes may favor particular applications (such as operation of anti-Stokes emitters) but it may be detrimental as in the case of RE based lasers because interactions among the active ions contribute for the increase of the laser threshold. In particular the study of ET processes in glasses having frequency gap in the visible region deserves large attention because when doped with RE ions some glasses may present efficient visible luminescence. Visible and infrared (IR) emissions of RE ions in glasses and glass-ceramics are known to be applicable in solid state lasers and broadband communications, respectively [17].

Many efforts have been done to enhance the intensity and gain of emissions in RE-doped glasses. First, it was reported that increment of concentration of REs in the system could intensify the Stokes and/or anti-Stokes luminescence intensities. However, a quench is observed often, after the introduction of 1–2 mol% of the RE ions [18, 19]. This happens due to further energy transfer among the RE ions, which results to increase the lifetime. Another approach was demonstrated to increase the absorption cross section of REs by introduction of second dopant, commonly trivalent ytterbium ions. The tripositive ytterbium ion shows large absorption cross section, therefore the large concentration of Yb^{3+} in vicinity of Er^{3+} provide larger absorption and emission gain, through energy transfer from $\{^2F_{5/2}$: $Yb^{3+}\}$ to $\{^4F_{7/2}$:$^4F_{9/2}$:$Er^{3+}\}$ [20]. In order to overcome such deficiencies, it has been demonstrated that metallic nanoparticles (NPs) may enhance the RE luminescence doped glasses and improve their nonlinear optical properties [21, 22]. In majority of the

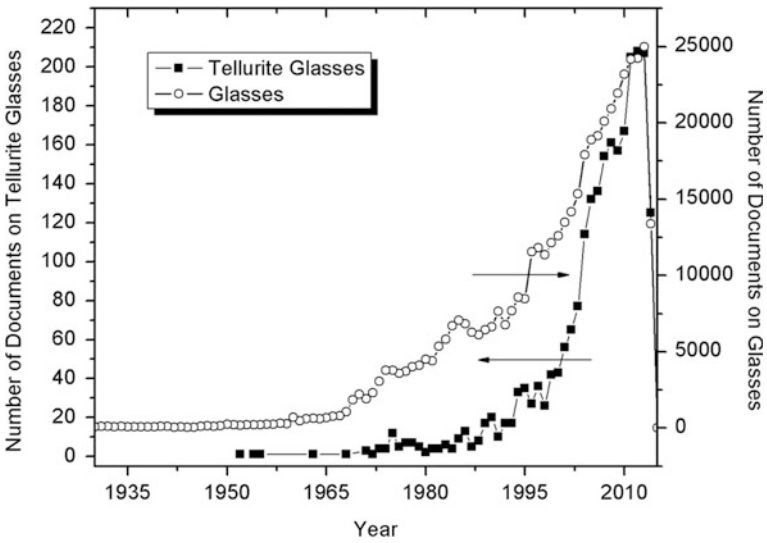

Fig. 14.1 Number of Scopus-index publications on glasses and tellurite glasses (Data taken from Scopus on 15 July 2014 [14])

studies, the presence of NPs contributes to enhance the material's luminescence efficiency either due to ET from the NPs to the RE ions or by influence of the large local field on the RE ions positioned in the vicinity of the metal. Indeed, the presence of nanostructures in the glass alters the luminescence efficiency. It is expected that RE doped glassy systems may be optically and thermally optimized by appropriate doping with metallic NPs.

14.2 Trivalent Rare Earth Ions Doped Glasses

Rare earth ions with their exclusive unfilled 4f shells are promising dopants in glasses to obtain optical fibers and solid state lasers [17]. At the atomic number of 57, 5s and 5p shells are full and 4f is unfilled. By increasing the atomic number in lanthanide group, the radius of 4f shell decreases gradually [23]. The outer 5s and 5p shells shield the 4f electrons and sensitize their environment so that several laser transitions are available in RE ions. For instance, there are 11 electrons in trivalent erbium ions (Er^{3+}:[Xe]$4f^{11}$), and 12 in Tm^{3+} ions. The schematic energy level of Er^{3+} ion is shown in Fig. 14.2. Russell-Saunders symbols ($^{2S+1}L_J$) are used to label the energy levels, where L, S and J are the orbital angular, spin angular and total angular momentums, respectively.

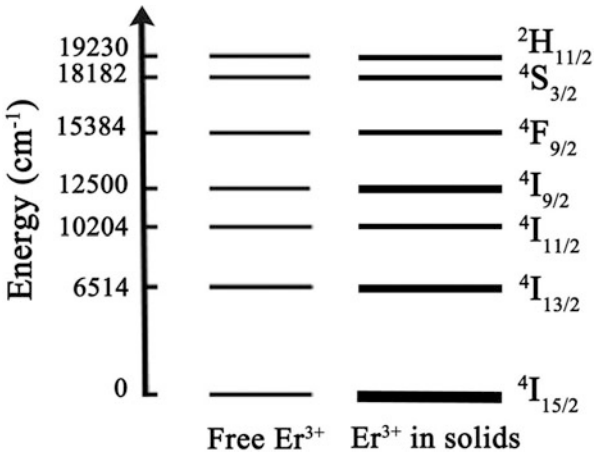

Fig. 14.2 Energy level of free-Er^{3+} ions and Er^{3+}-doped in a solid medium

Energy levels of rare earth ions can be explained by following Hamiltonian operator [24]:

$$H = H_{free-ion} + H_{"Crytal-field"} \tag{14.1}$$

where

$$H_{free-ion} = -\frac{\hbar^2}{2}\sum_{i=1}^{N}\nabla_i^2 = \sum_{i=1}^{N}\frac{Z^* e^2}{r_i} + \sum_{i<j}^{N}\frac{e^2}{r_{ij}} + \sum_{i=1}^{N}\zeta(r_i)\vec{s}_i.\vec{l}_i + negligible\ terms. \tag{14.2}$$

Here, N is the number of electrons in 4f, Z^* is the effective nuclear charge, including the inner electrons and nuclei, $\zeta(r_i)$, s_i and l_i are the spin-orbit coupling efficiency, and spin and orbit angular momentum, respectively. The terms in this equation (from left to right) define the kinetic energy, Coulomb interaction, mutual Coulomb repulsion and spin-orbit interaction of the 4f electrons. The last two terms are responsible for the broadening of energy level structure of RE ions in a host, which lift the degeneracy of the $4f^N$ electron configuration. A non-spherical symmetric crystal field in solids splits the energy levels of ion, which is frequently called as "Stark splitting". Due to shielding by 5s and 5p electrons, the crystal field Hamiltonian is 100 times weaker than electrostatic and spin-orbit interactions, in 4f electrons [24]. It is worth to mention that electric-dipole intra $4f^N$ transitions are forbidden due to matching parity of all levels, however they became allowed as a result of mixture into the $4f^N$ configuration of a small amount of excited opposite parity configuration.

In the presence of magnetic field, and considering the ion-ion interaction, two more terms will be added into the Eq. 14.1

$$H = H_{f-ion} + H_{CF} + V_{EM} + V_{ion-ion} \tag{14.3}$$

where V_{EM} is the Hamiltonian of interaction of light by ion, and the last term represent the interaction of two neighboring ions. V_{EM} is responsible for absorption transitions, when frequency of incoming magnetic field is in resonance or near-resonance with transition between different energy levels of RE ions.

The efficient emission intensity of REs embedded in glasses is limited to particular concentration so that further introduction of REs results in clustering of dopants or inefficient energy transfers. The formation of such clusters increases the nonradiative transfer rates between REs; therefore "concentration quenching" phenomena may occur [19, 25]. Several methods have been proposed to avoid the quench phenomena by increasing the efficiency of RE emissions. Enhancements through the effect of co-dopants on local symmetry of RE, adjusting the local interaction with suitable crystal structure, reduction of quench centers, semiconductor induced ET and introduction of noble metallic NPs are some of appropriate proposals [26].

14.2.1 Radiative Properties and Judd-Ofelt Theory

Judd [27] and Ofelt [28], independently and simultaneously formulated the theory of absorption and emission of lanthanides. Interestingly, approaches, assumptions and results of both theories were one and the same; however there are some differences in definitions. Judd defines the theory as the optical absorption while Ofelt referred to crystal spectra of RE ions [29]. Judd-Ofelt theory defines the properties of the radiative transitions in REs. Using this theory, radiative transition probabilities, branching ratios and intrinsic lifetime of an excited state to its lower states can be determined by assessing the three intensity parameters, Ω_i ($i = 2, 4$ and 6). The calculated oscillator strength (f_{cal}) of an electric-dipole absorption from the ground state $/(S,L)J>$ to the excited state $/(S',L')J'>$ depends on the Judd-Ofelt intensity parameters by

$$f_{cal}\left[(S,L)J;\left(S',L'\right)J'\right] = \frac{8\pi^2 mc}{3h\lambda e^2(2J+1)}\left[\frac{(n^2+2)^2}{9n}S_{ed} + n^3 S_{md}\right] \tag{14.4}$$

where α is the absorption coefficient (cm^{-1}), N is the number of active ions (mol. L^{-1}), e, m, c, h and λ have their common definitions in physics. Here, S_{ed} and S_{md} are electric dipole and magnetic dipole linestrenghts, respectively.

$$S_{ed} = e^2 \sum\nolimits_{t=2,4,6} \Omega_t \left|\left\langle (S,L)J \middle\| U^{(t)} \middle\| \left(S',L'\right)J' \right\rangle\right|^2 \tag{14.5}$$

$$S_{md} = \frac{e^2\hbar^2}{4m^2c^2}\left|\left\langle (S,L)J\middle\| J\vec{L} + 2\vec{S}\middle\|\left(S',L'\right)J'\right\rangle\right|^2 \tag{14.6}$$

Thus, three intensity parameters can be evaluated by a least square fitting to equalize the calculated and experimental (f_{exp}) oscillator strengths,

$$f_{exp} = \frac{4.318 \times 10^{-9}}{N}\int \alpha(\omega)d\omega \tag{14.7}$$

The reduced matrix elements, $\|U^{(t)}\|^2$ ($t = 2$, 4 and 6) [30, 31] are consistent from host to host, and Ω_t ($t = 2$, 4 and 6) are known as Judd-Ofelt intensity parameters that can be estimated by a least-square fitting method of experimental oscillator strengths on calculated ones. Magnetic dipole term is resulted from orbit-spin coupling and its different probabilities, considering the selection rules, are discussed and given in Ref. [32]. The transition probabilities A, branching ratio β and radiative lifetime τ can be calculated by

$$A_{J\to J'} = \frac{64\pi^4}{3h(2J+1)\lambda^3}\left[\chi S_{ed} + n^3 S_{md}\right] \tag{14.8}$$

$$\beta = \frac{A_{J\to J'}}{\sum_{J'} A_{J\to J'}} \quad \text{and} \quad \tau = \frac{1}{\sum_{J'} A_{J\to J'}} \tag{14.9}$$

The Judd-Ofelt intensity parameters of Er^{3+} ions in different glassy hosts are tabulated in Table 14.1. The lifetime of excited states of RE ions is an important parameter that defines the possibility of achieving the population inversion and efficiency of pumping in amplifiers and laser applications. For a particular excited sate, transition rate is given as inverse of the lifetime. Transitions from a state include both radiative and NR decays. Radiative transitions are due to absorption and emission of a photon, while nonradiative transitions correspond to the interaction of ions with lattice quantized network; the phonons and energy transfers etc. Nonradiative decay rates from excited states play a significant role to choose the suitable host for different applications. For example, multi-phonon (MP) relaxation rate in borate and phosphate glasses in $^4I_{11/2}(Er^{3+})$ excited states is large which reduces the radiative emissions and quantum efficiency of $^4I_{13/2}(Er^{3+})$ excited state. On the other hand, tellurite glass possesses lower phonon energy which is favorable to enhance the lifetime of $^4I_{11/2}$ level in Er^{3+}; therefore, the efficiency of the tellurite glass is large enough to develop the erbium doped fiber amplifiers (EDFA), pumping at 980 nm, as well as solid state upconverters.

The RE-doped glasses have many technological applications. They can be used as solid state lasers, sensors, optical fibers, amplifiers and etc. It is just at 1961 that Snitzer [36] reported the first fiber prepared by Nd^{3+} ions in solid state flash lamp pumped laser, which operates at 1061 and 1062 nm. In 1969, Koester and Snitzer reported on the near single-Nd^{3+}-doped fiber laser. Kao and Hockham [37] developed the theory of propagation in core-clad fibers and studied the structured optical

Table 14.1 Judd-Ofelt parameters of the Er^{3+} ion in various glasses ($\times 10^{-20}$ cm^2) [33]

Glass type	Ω_2	Ω_4	Ω_6	Ω_4/Ω_6
Silicate	5.59	1.42	0.87	1.63
Phosphate	4.67	1.37	0.77	1.78
Tellurite	5.34	1.75	0.94	1.86
Germanate	5.72	0.91	0.32	2.84
Fluoride	2.91	1.27	1.11	1.14
Borate [34]	4.11	1.45	1.42	1.02
Phospho-tellurite [35]	4.25	1.50	0.43	2.44

fiber. In 1972, Sandoe et al. [38] reported the first phosphate glass containing Er^{3+} ions which emits at 1530–1560 nm regions. In addition, Stone and Burrus [39] studied the 800 nm emission of Nd^{3+} fibers (CW laser). Mears et al. presented the first tunable and Q-switched fiber laser which operates in two regions; 1528–1542 nm and 1544–1555 nm. First Transatlantic fiber optic TAT-8 cables were developed in 1990 and later Svendsen developed the optical network WDM system and he installed this system for the first time on long-haul routes in Norway on 1997 [40].

Broad and flat stimulated emission cross-section in communication band and large amplifications gain in L-band of Er^{3+}-doped tellurite glass, introduced them as promising materials for broadband applications. The cross-section of this broadband in heavy metal oxide glasses such as bismuth and tellurite glasses (having refractive index >2 and low phonon energy) is larger than phosphate, silicate and fluoride glasses (see Table 14.2). Solubility of RE ions is another factor to select the suitable host matrix. The solubility of a dopant directly depends on the strength of the structural bonding. For instance, in silicate glass four oxygen atoms are tightly bounded to silicon atom by the strong covalent linkages. Therefore, the incorporation of RE ions in silicate glass is weak, and uniform distribution is difficult. Due to this fact, remarkable amount of modifiers (usually alkalis) are required to break the covalent bonds, weakening the network structure and to form the non-bridging oxygens (NBO) [41]. Phosphate glasses are also based on tetrahedral structure. However their covalency is five. The double bond between phosphorus and oxygen increases the number of NBOs. Therefore phosphate glasses show better spectroscopic properties and emissions than silicates when doped with REs [42]. On the other hand, tellurite glass shows a 2-dimensional system, where the Te-O linkage is significantly weaker than Si-O bond in silicate glass. Thus, it is much easier to break the atomic network of tellurites. Moreover, the atomic/ionic diameter of Te is larger than Si, therefore the network is not tightly closed. The open and weak network in tellurite glass facilitates the incorporation of RE ions and formation of uniform doped glasses is easier than silicate and phosphate glasses [43].

Table 14.2 Full-width at half maximum, emission cross-section and lifetime of 1.5 μm broadband of Er^{3+} ion in different hosts (AFP stands for alumina fluorophosphates) (All data taken from [44])

Glass	FWHM (nm)	σ_e ($\times 10^{-20}$ cm^2)	FWHM $\times$ σ_e	Lifetime (ms)
AFP	53	0.60	3.18	7.6–8.4
Silicate	40	0.55	2.2	5–8
Phosphate	37	0.64	2.37	6–10
Tellurite	65	0.75	4.88	2.5–4
Bismuth based	79	0.70	5.54	1.6–2.7

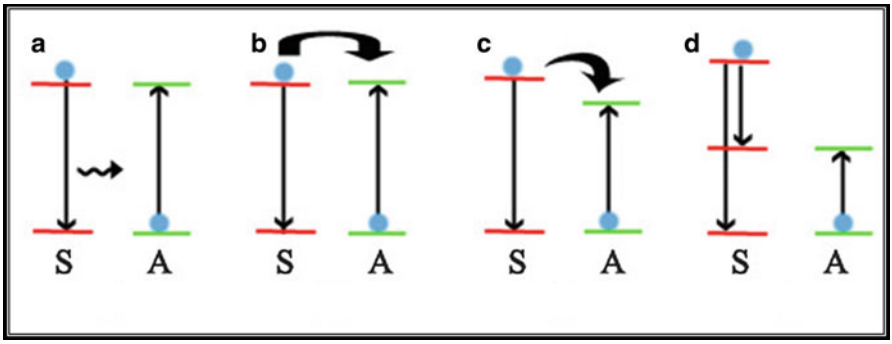

Fig. 14.3 Different energy transfer processes from a sensitizer (S) to an activator (A) in its ground state. Resonant radiative transfer (**a**), resonant energy transfer (**b**), Energy transfer assisted by phonons (**c**), and example of quenching of the fluorescence of *S* by energy transfer to *A* (**d**)

14.2.2 Energy Transfers and Cooperative Process

The neighboring active ions in short distances can interact with each other in two different approaches, (i) by summing up the photon energy by energy transfer (ET), and (ii) cooperative effects due to emission, absorption or sensitization. Given in Fig. 14.3 is the first proposal of the energy transfer processes, where activator ion is in its ground state and sensitizer ion is in an excited state.

Auzel introduced the situations when activator ion is excited, considering the exchanging of energy due to difference between ions energy, not only absolute energy [45]. He also presented and discussed different 2-step absorption, 2-photon excitation, cooperative luminescence, second harmonic generation (SHG), and cooperative sensitization. Cooperative upconversion (CUC) includes both cooperative sensitization and cooperative luminescence mechanisms. In high concentration of rare earth ions, the interaction between two electric dipole moments of ions is effected by short distance neighboring. CUC depends greatly on pumping intensity and concentration of ions. At low laser intensity, the CUC is not efficient. Cross-relaxation process is the reverse mechanism of CUC as shown in Fig. 14.4. The transition of two electrons in high and low energy levels leads to populate the

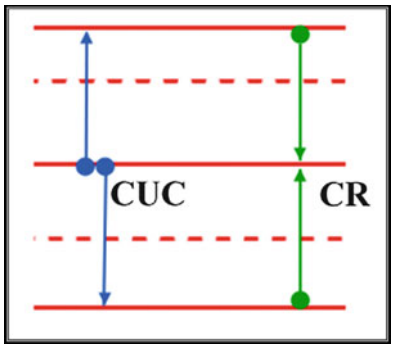

Fig. 14.4 Cooperative upconversion and cross-relaxation process in a schematic energy levels diagram of rare earth ions

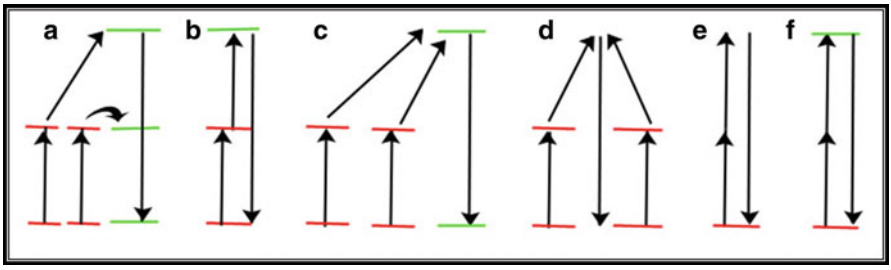

Fig. 14.5 Schematic energy transfer mechanism for different two photon upconversion processes. APTE effect in YF_3:Yb:Er (**a**), 2-steps absorption in SrF_2:Er (**b**), cooperative sensitization in YF_3: Yb:Tb (**c**), cooperative luminescence in Yb:PO_4 (**d**), Second harmonic generation in KDP (**e**), and 2-photon absorption excitation in CaF_2:Eu^{2+} (**f**)

middle energy state. Second-order cross-relaxation of excited levels is negligible due to low concentration of ions, in this excited state.

14.2.3 Non-linear and Upconversion Processes

Excited state absorption or 2-step absorption is shown in Fig. 14.5. An ion in its metastable level can absorb a second photon and be excited to higher energy levels. Normally, nonradiative decays through multi-phonon relaxations will help to populate lower metastable levels where the absorption of second or third photons may excite the ion, gradually.

The so-called "energy transfer" up-conversion is the general form of Dexter energy transfer [46] when the activator is in a metastable excited state. In a Dexter ET process, two ions, or two molecules or two parts of a molecule mutually swap their electrons. Increasing the distance between two particles result in an exponential decrease in the rate of process. This exchange mechanism is also named as "short-range" energy transfer. In addition, the interaction of activator and sensitizer should be weaker than the vibronic interaction of two parties. The latest circumstance, suggest the coupling of

single-ion level to the host network. By and large, this situation is more probable in high-concentration of REs in glass or crystal, where the splitting of pairs' level is as small as 0.5 cm^{-1} [47]. Besides, the transfer probability of such ET processes must be faster than radiative and nonradiative transitions from the metastable level. Therefore, two or three photons lead to generation of only one metastable state ion. The excited state absorption depends strongly on the pump intensity.

14.3 Optical Properties of Metallic Nanoparticles

Starting from early 1980, the field of nanoscience has been rapidly extended. It is a branch of science which deals with phenomena of 1–100 nm scales. Many basic sciences such as chemistry, physics, materials science, medicine, biology and also engineering are subjected with nanoscience and nanotechnology applications. The term, nanotechnology is the knowledge of produce, control and operate such small-sized particles to create noble materials, applicable for different area of science. Small particles firstly were used to color the metallic or glassy decorative subjects during the mediaeval times [48]. Lycurgus cup is an ancient Roman artifact – which relates to the fourth century – are appeared red in transmission and pale green in reflected light, due to incorporation of gold or silver or an alloy of both (average sizes of ~70 nm) [48]. In a scientific effort, initially Faraday (1857) studied the colloidal gold to determine the origin of its red color in compare to yellowish bulk gold [49]. However, it is just in recent decade that nanotechnology emerged as a basic and important science to develop scanning probe microscope and scanning tunneling microscope (STM) [50, 51] to study the isolated nanoclusters. In 1980, the first clusters of alkali metals with hundred atoms were produced and studied [52]. Present nanoscience techniques aimed to study the catalysts and to optimize the reaction rate, which reduce the iteration of experiments by trial and errors. More recently, nano-biology and nanomedicine used the nanoscience to overcome the cancer cells [53] and solid tumors [54]. Data storages with high capacity are developed by tunneling of the magnetization of a cluster through a magnetic anisotropy barrier [55].

The shape and the size of NPs affect their optical properties, such as surface plasmon resonance (SPR) absorption band position and shape [56]. By and large, formation of non-spherical metallic NPs results in red-shift of SPR peak and changes its Gaussian shape. Practically, any desirable shape of NPs can be created, such as nano-rods, nano-wires, nano-cages, aggregates, nano-prisms, nano-spheres, nano-sheets and plates [57–59] which show different absorption spectrum and optical properties. Complicated structures like nano-prisms and aggregates showed broad spectrum peaks due to large non-degenerate resonance modes. The non-degeneracy increases with lowering the symmetry of system [60]. Besides, the size of NPs, refractive index of environment medium and other proximal NPs are important factors to determine the SPR band. Therefore, the chief challenge is to optimize the optical properties of nanostructure by adjusting the frequency, FWHM, and shape of the SPR absorption band as shape, size, dielectric function, electron density and effective mass of nanoparticles changes.

14.3.1 Interaction of Light with Nanoparticles

The study of optical properties of metallic nanoparticles interacting with light has rapidly grown and become known as plasmonics [61, 62]. Nanoparticles undertake diverse response under the excitation by light due to scattering or absorption of photons. The photons with efficient energy can either excite the electrons by an internal electronic transition (optical absorption) or ionize the particle by emitting an electron from NP at high energy levels (photoemission spectroscopy). The absorption takes place due to SPR in the particles with sizes d, where $d << \lambda$, and λ is the wavelength of excitation light. The electrons of the metal are subjected into the electric field of incoming light which relocates them with respect to positive charge of nuclei. On the other hand, static Columbic force between positive and negative charges resist to this shift. Therefore, electrons of metal begin to oscillate. The resonant phenomena, typically is determined with a peak in visible region of absorption spectrum. Mie used the classical concept of dielectrics to develop a theory based on this behavior [63]. If the particle is not spherical, the absorption spectrum will be complicated (Fig. 14.6).

Gustav Mie developed the theory on the interaction of NPs with light [63]. Strong absorption band accompanies temperature increment of the particle. Large enhancement of the electric field in particle and its adjacent environment can be observed by near resonance excitations. Optical properties of metallic NPs strongly depend on the dielectric function of the host matrix (environment). The optical properties of a metal can be described by a simple Drude-Lorentz-Sommerfeld model [64]. The effect of an external field $E = E_0 exp(-i\omega t)$ on an electron with mass, m and charge, $-e$, can be written as

$$m\frac{d^2\vec{r}}{dt^2} + m\Gamma\frac{d\vec{r}}{dt} = -e\vec{E} \tag{14.10}$$

where Γ is the damping constant which is metal-dependant parameter. The polarization is $\vec{P} = -ne\vec{r}$, where n is the density of the electrons. Dielectric function, thereby, is given as

$$\varepsilon = 1 + \frac{4\pi P}{E} \tag{14.11}$$

in cgs system. Dielectric function is related to frequency as follow

$$\varepsilon = 1 - \frac{\omega_P^2}{\omega^2 + i\Gamma\omega} \tag{14.12}$$

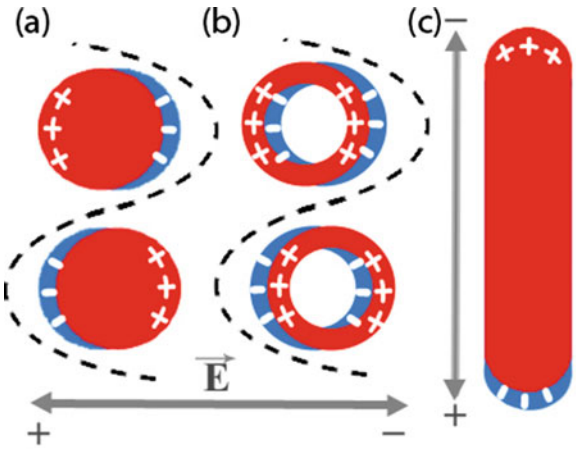

Fig. 14.6 Schematic interaction of light with metallic particles (surface plasmon resonance) for spherical nanoparticles (**a**), hallow nano-spheres (**b**) and nano-rods (**c**) [61]. In addition, this figure exhibits the increase number of resonant modes with decreasing the symmetry

where ω_P is the frequency of plasma,

$$\omega_P^2 = \frac{4\pi n e^2}{m} \tag{14.13}$$

Dielectric function is intrinsically an imaginary function, $\varepsilon = \varepsilon_1 + i\varepsilon_2$, where

$$\varepsilon_1 \approx 1 - \left(\frac{\omega_P}{\omega}\right)^2 \quad \text{and} \quad \varepsilon_2 \approx 1 - \left(\frac{\omega_P}{\omega}\right)^2 \frac{\Gamma}{w} \tag{14.14}$$

for damping constant smaller than frequency, $\Gamma << \omega$. The absorption coefficient is given by $= 2\omega k/c$, where $n + ik = \varepsilon$. In the case of clusters, the nuclei are static and electrons are assumed to move freely in an external field. For the particle sizes smaller than wavelength of light, at any time, the electric field is uniform around the cluster. For a cluster embedded in a medium, the electric field inside the cluster is

$$\frac{E}{E_0} = \frac{3\varepsilon_m}{\varepsilon + 2\varepsilon_m} \tag{14.15}$$

where E_0, ε and ε_m are the static electric field, dielectric constant of the sphere cluster and dielectric constant of medium, respectively. Mie frequency is defined as

$$\omega_M^2 = \frac{\omega_P^2}{1 + 2\varepsilon_M} \tag{14.16}$$

Having the volume of the particle V_p, the extinction cross section for a particle is

$$\sigma_{ext} = 9\varepsilon_m^{3/2}\left(\frac{\omega}{c}\right) V_p \frac{\varepsilon_2}{(\varepsilon_1 + 2\varepsilon_m)^2 + \varepsilon_2^2} \tag{14.17}$$

According to Mie [63], in a medium with refractive index, n, containing the NPs smaller than excitation wavelength, λ, the absorption coefficients can be determined by free electron approximation as

$$\alpha = \frac{9\pi p n^3 c\lambda^2}{\sigma_{dc}\left[\left(\lambda_m^2 - \lambda^2\right)^2 + \lambda^2 \frac{\lambda_m^4}{\lambda_a^2}\right]} \tag{14.18}$$

where p, σ_{dc}, c and λ_m are the volume fraction of the metal spheres in the glass matrix, the dc electrical conductivity, the velocity of the light, and the wavelength at maximum absorption, respectively. Reduced length scales are defined as

$$\lambda_a = \frac{2\lambda_c^2 \sigma_{dc}}{c} \quad \text{and} \quad \lambda_c = \frac{(2\pi c)^2 m}{4\pi N_c \varepsilon_m^2} \tag{14.19}$$

Here, m, N_c and ε_m are the electron mass, the number of electrons per unit volume and the complex form of dielectric function of metallic NPs. The wavelength at which the maximum absorption takes place is given as

$$\lambda_m = \lambda_c\left(\varepsilon_0 + 2n^2\right)^{1/2} \tag{14.20}$$

where ε_0 is the frequency dependent part of ε_m. FWHM of this band can be found as

$$FWHM = \frac{\lambda_m^2}{\lambda_a} = \frac{(\varepsilon_0 + 2n^2)c}{2\sigma_{dc}} \tag{14.21}$$

and the dc conductivity is given by

$$\sigma_{dc} = \frac{N_c e^2 L}{2mu_F} \tag{14.22}$$

where e, L and u_F are electron charge, diameter of NP and Fermi velocity.

$$u_F = \left(\frac{2E_F}{m}\right)^{1/2} \tag{14.23}$$

14.3.2 Preparation and Observation of Metallic Nanoparticles

There are several physical and chemical techniques to synthesize the NPs. One of the important physical techniques is to evaporate the metal from a source and deposit the gas on a substrate [65]. This method is more efficient since controlling the shape and size of the NPs are more facile. One of the important chemical

techniques is to reduce the metal ions or metal salts with a suitable reducing agent. This method is known as most suitable technique to produce the spherical NPs [57, 58, 66, 67]. For example, Xu et al. [68] embedded the silver NPs into the sodium-silicate glass through an ion exchange method and subsequent heat-treatments. There are also many other approaches such as electrochemistry techniques which are beyond the scope of this chapter [69].

Synthesis of the NPs includes two processes [70]: (i) formation of small seeds (nucleation) and (ii) growth process. The capping material plays an important role to determine the shape and size of NPs during the growth. If the capping material is very weak, the growth will continue to produce big crystallized particles. Contrary, if it is too strong, it may reduce or prevent the growth. Therefore, nanomaterial, capping material or reduction agent and medium are important factors to increase the efficiency of synthesize. Moreover, the concentration of agent is another factor to determine the concentration of initial seeds of metallic particles.

The clustering of the NPs can be discussed by following suggested models [71]:

(1) Coagulation process; in which the pairwise particles will be destroyed through the collisions and larger particles will be formed. In a simple model [72], by considering the identical probability of collision (K_D) for different particles, one can describe the coagulation process by

$$\frac{\partial Z_n}{\partial t} = -\frac{1}{2} K_D Z^2 \tag{14.24}$$

where, Z_n is the concentration of particles of kind n. The solution for given time evaluation equation is

$$Z(t) = \frac{Z_0}{1 + 0.5 K_D Z_0} \tag{14.25}$$

And the required time for coagulation is

$$t_c = \frac{2}{K_D Z_0} \tag{14.26}$$

For the coagulation of two particles with radius R_1 and R_2 and respective diffusion velocity of $u(R_1)$ and $u(R_2)$, the probability constant is:

$$K_D = \pi (R_1 + R_2)^2 [u(R_2) - u(R_1)]. \tag{14.27}$$

(2) Ostwald ripening process; in which the large particle will be grown through feeding by smaller particles. Therefore, the smaller particles start to vanish [73]. The matter in its thermodynamic balance consists of surrounding gaseous cloud. The bigger the particle is, the lower number of particles in cloud exists. The

diffusion from cloud to matter and vice versa is consistent with growth and disaggregation of particles, respectively.

(3) Coalescence of particles; in this process, the particles grow due to a strong chemical or physical bonding which is consistent with coagulation in first step and the consequent Ostwald ripening effect. The critical size of particle to grow or dissolve is [74]

$$r^* = \frac{2V\gamma}{3k_BTln(S_r)} \tag{14.28}$$

where V, γ and S are the molecular volume, surface free energy per unit surface area and saturation ratio. Therefore, for a given $S > 1$ and temperature (T), the particle with radius $r < r^*$ starts to grow, while the particles with $r > r^*$ will dissolve.

Properties of NPs are characterized by their extremely small size which needs appropriate apparatuses to be probed. The first instrument to observe the NPs is usually UV-Vis absorption spectroscope since NPs show strong absorption peak at near-UV to near-infrared region. Up to now, many instruments were developed to characterize/observe the structure of NPs such as X-Ray diffraction (XRD), atomic force microscopy (AFM), scanning electron microscopy (SEM), transmission electron microscopy (TEM), X-Ray absorption spectroscopy (XAS) and its fine extended device (EXAFS), dynamic light scattering, energy dispersion X-ray (EDX), IR and Raman [75–77].

XRD technique can be used to determine the crystalline phases, average inter-particle distances, and atomic structure of the nanoclusters. The size of particles, defects and strains of nanocrystals can be defined by measuring the width of diffraction lines. The broadening of the diffraction linewidth is directly related to reduction of nanocrystal size.

AFM, STM, and chemical force microscopy are usually called in a group named: the scanning probe microscopy (SPM). It can be applied on versatile organic and inorganic materials in their gassy or liquid phases. AFM captures the image of specimen through the difference between the atomic forces in short-range and long-range which are repulsive and attractive, respectively [78]. Scanning force microscopy (SFM) also is a useful tip to measure the electrostatic and magnetic interactions between the molecules. SEM is another commanding technique to observe the surface of any type of materials with a resolution of 1 nm [77]. The principle of SEM is based on the interaction of incoming electron with the sample, which will be captured by its backscattered electron. Therefore, both structural and topological properties can be defined through two captured beams.

TEM is also another powerful instrument to characterize the chemical composition and spatial structure [76]. Recently, high-resolution-TEM is developed which allow the imaging of crystals as small as 1 Å. TEM is usually used to determine the shape, size, crystallinity and inter-particle interactions in nanomaterials.

14.3.3 Surface Enhanced Raman and Fluorescence Spectroscopy (SERS, SEFS)

Raman spectroscopy is a powerful technique to study the vibrational modes of molecules through an elastic scattering of a monochromatic excitation source in the routine range of 200–4000 cm^{-1}. Molecular vibrations are either infrared (IR) and/or Raman active. Therefore, Raman technique is mainly used to complement the IR measurements. The critical issue in Raman spectroscopy is the small cross section which requires lot of molecules to achieve valuable results. The efforts to develop the detection ability by Raman spectroscopy have been yield to introduce the Surface-Enhanced Raman Spectroscopy (SERS) [79], where the enhancement factor up to $10^{10} \sim 10^{11}$ times may aim to detect single molecules [80–82]. The enhancement results from the enhanced localized electromagnetic field in the surface of metallic NP and dielectric environment. Furthermore, topological change of NPs in dielectrics adds promoted electric field by lightening rod effects (LRE) in non-spherical (elliptical, cube, pyramid shapes and so on) surface of NPs which enhances the intensity of scattered Raman beam up to 10^{14} times [82]. Messinger, Wang and Kerker developed the theory of the SERS [83, 84]. Fleishmann et al. [85] reported the first SERS using roughened metal electrodes.

The enormous localized electric field between two NPs, firstly, enhances the excitation light, and as the result, the Raman modes of probing molecular will enhance by a factor of η^2, where η is the enhancement factor. Moreover, the emitted Raman signals experience further enhancement by same SPR effect. Therefore, output Raman signal is enhanced by a factor of η^4 [86]. The maximum enhancement happens near the plasmon frequency (ω_P) [87]. Even if, the plasmon resonance may not be efficient in special cases, LRE aims to confine the large electric field in the sharp edges of metal surface or at curved surfaces.

The SERS effect is reported for the first time in a glassy system by Dousti et al. [88]. The incorporation of silver NPs as small as 12 nm into the zinc tellurite glass increases the Raman signals as large as eight times. However, controlling the resonance frequency, shape and size of the NPs is still a controversial subject which effectively determines the enhancement factor. For instance, the addition of concentration of NPs can result in a red shift of SPR band and evolution of enhancement factors of Raman and photoluminescence (PL) signals [89].

On the other hand, the presence of metallic NPs in vicinity of luminescent centers can alter the radiative emission properties of such dopants, so called surface enhanced fluorescence spectroscopy (SEFS). Large electromagnetic field can be localized in vicinity of the metallic NPs. Therefore, they can trap the photons (photon catchers). One of the advantages of such system is fluorescence enhancements due to controlling the light and enhancing the local field around the fluorophores. Such enhancement by SPR was firstly reported by Malta et al. [21]. The application of SEFS on RE-doped glasses containing noble metallic NPs shows significant results which are promising to develop the optical amplifiers, solid state lasers, color displays and versatile nanophotonics devices [90–92].

The enhancements of emissions in the hosts containing metallic NPs with average size of D and separated by the distance d, are mainly attributed to enlarged local electric field. The enhancement factor η, of the system can be evaluated by

$$\eta = \frac{E_{loc}}{E_i} = \frac{(D+d)}{d} \tag{14.29}$$

where E_{loc} and E_i are the amplified local field (effective field, E_{eff}) and the incident field, respectively [62]. The effective field is interpreted by Malta et al. [21] as

$$\vec{E}_{eff} = (\varepsilon_0 + 2)\left[1 + \frac{q\omega_p^2}{3\varepsilon_0\left\{(1-q)\left(\omega_p^2/3\varepsilon_o\right) - \omega^2 + i\gamma\omega\right\}}\right]\frac{\vec{E}_0}{3} \tag{14.30}$$

where ε_0 is the dielectric constant in the presence of external electric field E_0, and γ is the damping coefficient of plasmon resonance.

Radiative decays of any fluorophore (e.g. RE ions) can be modified by plasmonics approach. Various shapes, sizes, corresponding local field of metallic NPs and distances between the fluorophore and NP can result in different enhancement order of emissions and quantum efficiency. Modification of radiative decay is usually called as "radiative decay engineering" [62]. In the next section, we review some of the available reports on the optical properties of the rare earth doped oxide glasses containing metallic nanoparticles.

14.4 Rare Earth Doped Glasses Embedded with Metallic NPs

Glasses are superior candidates to embed the RE ions and metallic NPs due to their high transparency, mechanical strength, and simple preparation in any size and shape and high energy stretching vibration which extinct the interaction of ligand with metals. Therefore, metallic glasses composites containing nanoclusters or NPs are introduced as potential substrate materials (hosts) for significant local field enhancement to increase the luminescence of RE ions [90, 93–95]. Moreover, the introduction of metallic NPs may modifies the thermal and structural properties as well as chemical durability of oxide glasses [96, 97], which are beyond the scope of this chapter. Thermal features of glasses can be also modified by incorporation of metallic NPs and may result in considerable increase in thermal diffusivity and thermal conductivity [98]. This is particularly important considering that cooling is one of the most challenging technical issues to be overcome in the areas of microelectronics and solid-state lighting. It has been reported that the thermal diffusivity of materials doped with metallic NPs depends on the size and concentration of NPs, even though the subject is still a matter of controversy in the literature. The large nonlinear absorption of silver nanoclusters and NPs are

recently reported in the silicate, borate and oxyfluoride glasses, which are promising for applications in optical limiting and object's contrast enhancement due to the non-saturated and saturated nonlinear absorptions [99–101].

The formation of NPs in the glass commonly carries out by thermodynamic reduction of NPs in the presence of an oxidant agent. Som and Karmakar showed the feasible reduction process of silver [90] and gold [95] in antimony glass, as follows

$$Sb^{5+}/Sb^{3+},\ E^0 = 0.649\ V \tag{14.31a}$$

$$Au^{3+}/Au^0,\ E^0 = 1.498\ V \tag{14.31b}$$

$$Ag^{+}/Au^0,\ E^0 = 0.7996\ V \tag{14.31c}$$

$$3Sb^{3+} + 2Au^{3+} \rightarrow 3Sb^{5+} + 2Au^0, \Delta E^0 = 1.05V \tag{14.31d}$$

$$Sb^{3+} + 2Ag^{+} \rightarrow Sb^{5+} + 2Ag^0, \Delta E^0 = 1.02V \tag{14.31e}$$

They suggested that the reduction of gold is faster than the silver ions. This idea led to preparation of $gold_{core}@silver_{shell}$ nanoparticles [102]. Wu et al. [103] investigated the reduction of silver ions to neutral NPs in a bismuth-borate glass system, and the possible reduction is proposed as

$$Bi^{3+}/Bi^0,\ E^0 = 0.3172\ V \tag{14.32a}$$

$$Ag^{+}/Ag^0,\ E^0 = 0.7996\ V \tag{14.32b}$$

$$Bi + 3Ag^{+} \rightarrow Bi^{3+} + 3Ag^0, \Delta E^0 = 2.0816V \tag{14.32c}$$

Dousti et al. [104] illustrated the reduction of silver ions to silver NPs in Er^{3+}-doped zinc tellurite glass. The reduction of Ag^{+} particles to Ag^0 NPs can be discussed by the reduction potential (E^0) of redox system elements. The E^0 values of each component in this system are:

$$Te^{6+}/Te^{4+},\ E^0 = 1.02\ V \tag{14.33a}$$

$$Ag^{+}/Ag^0,\ E^0 = 0.7996\ V \tag{14.33b}$$

$$Er^{3+}/Er^0,\ E^0 = -2.331\ V \tag{14.33c}$$

$$Er^{3+}/Er^{2+},\ E^0 = -3.0\ V \tag{14.33d}$$

Probable reduction process and their total potentials are as following:

$$Te^{4+} + 2Er^{3+} \rightarrow Te^{6+} + 2Er^{2+} \qquad \Delta E^o = -7.02 \tag{14.34a}$$

$$3\ Te^{4+} + 2\ Er^{3+} \rightarrow 3\ Te^{6+} + 2\ Er^0 \quad \Delta E^o = -7.722 \tag{14.34b}$$

$$Te^{4+} + 2\ Ag^{+} \rightarrow Te^{6+} + 2\ Ag^0 \quad \Delta E^o = +0.5792 \tag{14.34c}$$

Therefore, from the thermodynamic point of view, only the last redox reaction (14.34c) is feasible. The reduction of Ag^{+} ions to Ag^0 neutral particles and growth

of silver NPs are also reported by addition of other reducing agents such as SnO [105].

In the past decade, there were group of authors who contributed in the studies of effect of the metallic NPs on optical properties of RE-doped glasses, glass-ceramics and thin films. The effect of asymmetric silver NPs reduced in an antimony glass system is reported by Som and Karmakar [90], where intense SPR peak were probed in UV-Vis-IR absorption spectra. They concluded that the decrease in NP-NP distances by increasing the concentration of Ag NPs enhances the localized electric field and broadens the plasmon peak by a red-shift up to 1100 nm. The formation of NPs with different shapes and size ranging between 4 and 31 nm was discussed as an Ostwald's ripening process.

Upconversion of only Ag NPs (without any RE ion in system) is also reported by few authors [90, 106]. Som and Karmakar [90] presented the upconversion of Ag NPs on antimony glass under 798 nm excitation wavelength where the SPR band was observed around 598 nm in UV-Vis absorption spectrum. The upconversion emission wavelengths were located at ~536 and 654 nm. Dousti et al. [106] also observed same behavior of Ag NPs in tellurite glass while broad emission band centered at 500 nm originated due to 786 nm excitation wavelength. Luminescence of metallic NPs are also observed by different research groups [107]. Such radiative emissions from metallic NPs can either contribute to further enhance or quench of the neighboring luminescent ions through energy transfer mechanism.

14.4.1 Eu^{3+}-Doped

The introduction of metallic NPs into the glassy hosts was first reported by Malta et al. [21]. A large enhancement in the order of 5.6 for luminescence of Eu^{3+} in borate glass (emission at 612 nm and under 312 nm excitation wavelength) has been observed due to the presence of small silver particles by a concentration around 7.5 wt%. The absorption peak of small silver particles in this study showed a sharp peak at 312 nm. In 1999, Hayakawa et al. [108] reported on the enhanced luminescence of Eu^{3+} ions doped in silica glass in presence of Ag NPs having sizes of about 4.3 nm (surface plasmon band was observed at 394 nm). The enhancement of $^5D_0 \rightarrow {}^7F_J$ (J = 0, 1, 2, 3 and 4) emissions of Eu^{3+} ions doped borosilicate glass (derived by a sol-gel method) in vicinity of polymer-protected gold NPs is also reported by Hayakawa et al. [109], where 6 times enhancement is observed under a long UV excitation light.

The luminescence of Eu^{3+}-doped lead-tellurite glass embedding gold NPs were characterized by Almeida et al. [110]. The sample containing 0.5 wt% Au NPs and annealed for 41 h (average particle diameter ~4 nm) show largest enhancements in Eu^{3+} spectra under 405 nm excitation. Since, the electric dipole transitions such as $^5D_0 \rightarrow {}^7F_{4,2}(Eu^{3+})$ are sensitive to polarizability and environment around the RE, rather than those magnetic dipoles ($^5D_0 \rightarrow {}^7F_{1,3}$), the presence of metallic NPs alert them progressively. They concluded that the presence of small NPs cannot result in

to the energy transfer process, hence the main contribution for such intensification is attributed to increased local field around the Eu^{3+} ions. Such enhancements are also observed in Eu^{3+}-doped GeO_2-Bi_2O_3 glasses containing Au NPs by the same research group [111], where SPR band of NPs observed at 500 nm and contributes to 1000 % and 500 % enhancement of $^5D_0 \rightarrow {}^7F_{2,4}$ and $^5D_0 \rightarrow {}^7F_{1,3}$ emissions, respectively.

The luminescence enhancements of Eu^{3+}-doped zinc-tellurite glass and lead-tellurite glass are also reported. Two-times enhancement is observed for Eu^{3+}-doped ZnO-TeO2 [112] and PbO-TeO2 [113] glasses after 12 and 9 h of heat-treatments which lead to formation of silver NPs with an average size of 14 and 10 nm, respectively. Such enhancements are attributed to intensified local field in distances between NPs and RE ions, induced by surface plasmons. In both reports, the silver NPs are grown along (200) crystallographic direction (JCPDS no. 030931), as revealed by TEM images (lattice constant of about 2–2.05 Å).

Jimenez at al. also reported on the enhanced UV-excited luminescence of Eu^{3+} ions in silver/tin-doped glass [114]. However, such enhancements are attributed to Ag^+ ions, and not Ag NPs. Moreover, the quenched PL is caused by Ag NPs, by providing "the paths for the nonradiative loss of excitation energy in europium ions through coupling with plasmon resonance modes". Eu^{3+}-doped aluminosilicate glasses containing different Ag species are reported by Li et al. [115]. The observed broadbands in UV-Vis absorption, photoluminescence excitation and emission spectra of the glasses suggest the presence of Ag ions and molecular-like Ag species. However, after 30 and 120 min of heat-treatments, the silver NPs are formed in the glasses and are discussed in terms of following redox reaction; $Eu^{2+} + Ag^+ \rightarrow Eu^{3+} + Ag^0$. The surface plasmon band of the silver NPs in this glass is observed at 440 nm by taking the difference between absorption spectra of samples with and without NPs. Although the excitation lines of Eu^{3+} ions are suppressed in the spectra of Ag NPs-doped samples, the luminescence emissions in the visible region enhances under 350 nm excitation wavelength. The authors concluded that the observed enhancement can be purely associated to the energy transfer from silver aggregates to Eu^{3+} ions and not an enlarged local field by SPR of Ag NPs (Fig. 14.7).

Jiao et al. [116] investigated the effect of concentration of Eu^{3+} ions on the formation and growth of silver NPs. They concluded that increasing the Eu_2O_3 content led to increase the Eu^{2+} ions and increasing the concentration of Eu^{3+} ions and Ag NPs as; $Eu^{2+} + Ag^+ \rightarrow Eu^{3+} + Ag^0$. In this regard, the enhancement and quenching of Eu^{3+} emissions are observed under 280 and 340 nm excitation wavelengths, respectively. These results are in good agreement with Riano et al. [117] reporting on the intense surface plasmon band of Ag NPs in presence of Eu^{3+} ions, rather than Pr^{3+} ions. However, they observed quenching of the luminescence of Eu^{3+} ions, an indicative of energy transfer from Eu^{3+} ions to Ag NPs. Wei et al. [118] also worked on the preparation of Ag NPs-embedded Eu^{3+}-doped oxyfluoride glasses. The enhancement in emissions of Eu^{3+} ions are attributed to presence of silver NPs, small-molecular like silver and isolated Ag^+ ions under 464, 350 and 270 nm excitation wavelengths, respectively.

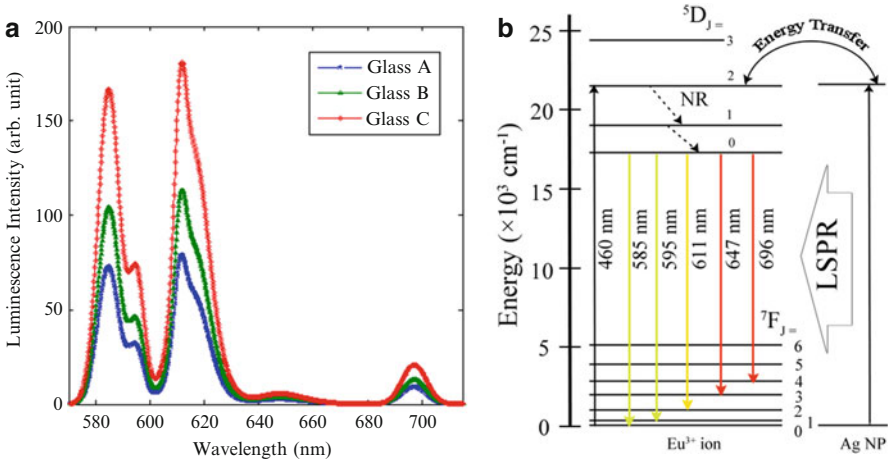

Fig. 14.7 (**a**) Luminescence spectra of Eu^{3+} ions in tellurite glasses embedding (A) 0 mol%, (B) 0.5 mol% and (C) 1 mol% silver nanoparticles (NPs) under 460 nm excitation wavelength. (**b**) Schematic partial energy level diagram of Eu^{3+} ions in vicinity of silver NPs showing localized surface plasmon resonance (LSPR), nonradiative (NR) and radiative decays (Figures are adapted from [113])

Kumar et al. reported on the enhancement of the luminescence of Eu^{3+}-doped titanosilicate glass by introduction of silver NPs [119]. The silver NPs with average particle size of 14.9 nm and TiO_2 polycrystalline are observed in SAED and XRD pattern of the glass samples. A broad absorption band in the 300–400 nm region is assigned to SPR band of NPs. The photoluminescence emissions ($\lambda_{exc} = 393$ nm) and excitations ($\lambda_{emi} = 612$ nm) showed enhancements after incorporation of silver NPs. The asymmetry ratio (AS, the ratio of integrated emissions bands of Eu^{3+} ions) are given as $(\int {}^5D_0 \rightarrow {}^7F_2\, d\lambda)/(\int {}^5D_0 \rightarrow {}^7F_1\, d\lambda)$, which varies by the addition of silver NPs due to modification of (i) ligand filed and (ii) refractive index around the RE ions. AS factor increases from 2.627 to 3.615 for singly-doped and co-doped samples, respectively.

Culea et al. [120] also reported on the effect of Ag_2O and Ag NPs on the spectroscopic and structural properties of lead-tellurite glasses. Enhancement of red-emissions of Eu^{3+} ions by Ag NPs is also reported in other medium [121] under a green light excitation which is known to be promising materials for solar cell and nano biotechnology. Moreover, white light emission is observed in Eu^{3+}-doped oxyfluoride glass containing molecular-like (ML) silver, where no proof was observed to attribute the enhancement of photoluminescence to plasmonic silver NPs [122].

14.4.2 Er^{3+}-Doped

In 2002, Strohhofer et al. [123] reported on the enhanced emission of Er^{3+} in a borosilicate glass by an ion-exchange process. They observed 70 and 220 times enhancements in broadband line under 488 and 360 nm excitation wavelength. They concluded that such enhancement can be attributed to the silver ions/atoms defects and an ET to Er^{3+} ions. Chiasera et al. [124] reported on the silver-sodium exchange process in soda-lime silicate glass containing Er^{3+} ions. The plasmon band of silver was observed in blue region, and its intensity increased by further heat-treatments. The silver exchange has no effect on the broadband emission of erbium; however, it increased the lifetime of this metastable state, which was in disagreement with some older reports [123, 125]. The increase in lifetime of $^4I_{13/2}$ was attributed to silver-induced radiation trapping [124], while the decrements is featured by silver-induced defects in glassy hosts [123, 125]. Using the gold NPs in an Er^{3+}-doped SiO_2 thin film, prepared by sol-gel method, the optical absorption and emission at 1.54 μm were characterized by Fukushima et al. [126]. One hundred times enhancement emissions of sample with 1 mol% Au NPs were attributed to strong filed originated from confined surface plasmon, while the excitation wavelength were selected to line in the Au plasmon band region, located at 520 nm. Lin et al. [127] fabricated the Au NPs-doped erbium optical fiber in a germane-silicate glass which showed plasmon resonance band around 498.2 nm, and the net gain of broadband emission at 1535.6 and 1551.2 nm experienced enhances under 980 nm excitation wavelength. The quenches are observed under 488 nm excitation wavelength and are attributed to absorption of the incident energy by Au NPs. They discussed the observed loss by an ET from Au NPs to lattice, and not to Er^{3+} ions. The effect of the temperature on XRD pattern, absorption and emission spectra and Judd-Ofelt parameters in a Er^{3+}-Au NPs co-doped alumina-silicate glass is investigated by Watekar et al. [128]. A blue shift in plasmon absorption band of gold NPs is observed by increasing the annealing temperature. The radiative lifetime and integrated emission cross-section of infrared emissions of Er^{3+} ion decreased after introduction of Au NPs. Such quenches in non-resonance excitation process is attributed to ET from Er^{3+} ions ro Au NPs. Singh et al. [129] studied the effect of annealing time interval on the size of Ag NPs in Er^{3+}-doped tellurite glasses. They exposed the samples containing Ag NPs under the temperature below the glass transition temperature for different periods of time. They observed increased size of NPs and enhancements in up-conversion emissions in visible range (green and red lines) by increasing the annealing time.

The introduction of Au NPs in Er^{3+}-doped antimony glass raise up to preparation of dichroic nanocomposite [95], showing different colors in transmittance and reflecting surfaces. The enhancements in the order of 3.4 and 7.5 times in green (536 nm) and red (645 nm) bands through an upconversion luminescence were attributed to the enlarged local field by asymmetric Ag NPs. Diffraction peaks of Au NPs in XRD pattern was in good conformity with SAED results for NPs with

sizes about 11–30 nm. Once more, broadening of plasmon peak (612–664 nm) was observed due to presence of non-spherical metallic NPs. They conclude that optimized upconversion intensity of Er^{3+}-doped antimony glass occurs with 0.03 wt% of Au. However, further increase of Au concentration results in quenched luminescence, showing the ET from Er^{3+} ion to Au NPs and reabsorption due to SPR of gold NPs [95].

Rivera et al. [130] showed that by exciting the Er^{3+} ions doped in tellurite glass containing silver NPs upon 980 nm laser, a blue shift occurs in the peaks of broadband emission (~1.55 μm). The modification of Stark energy levels (blue shift) was attributed to oscillator strengths of NPs which results in the ET from NP to Er^{3+} ions. The small SPR peaks were revealed in an Er^{3+}-free Ag NP-doped tellurite glass centered at 479 and 498 nm for 3 and 6 h annealed samples, respectively. The peaks in XRD pattern of tellurite glass containing silver NPs ($2\theta = 44.8 \pm 0.4°$, where $d' = 2.0231 \pm 0.0169$ Å) belongs to the (hkl – 200) diffraction planes of Ag crystals (JCPDS Card File No. 4–0783.). Slight increase in FWHM and intensity of broadband emission of Er^{3+} ion (~1.55 μm) were observed by increasing the annealing time interval. The lifetime of 1.55 μm decreases by introduction of Ag NPs in their system comparing to Er^{3+}-single-doped tellurite glass. In another study, Rivera et al. [131] showed that the lifetime of $^4I_{13/2}$ level increases due to presence of heat-treated gold NPs. Therefore, the upconversion luminescence ($^2H_{11/2} \rightarrow {}^4I_{13/2}$, 805 nm) upon the 980 nm excitation enhances drastically (~75 times) due to presence of annealed Au NPs up to 7.5 h. The large enhancement is attributed to LSPR of Au NPs which is located at 800 nm, as evidenced in UV-Vis-IR absorption spectrum, which modifies the local electric field through an electric coupling by Er^{3+} ions. The XRD peaks of Au NPs are revealed at $2\theta = 38.3 \pm 0.4°$ and $44.6 \pm 0.3°$, respectively corresponding to (111) and (200) diffraction planes of gold [131].

de Campos et al. [132] investigated the Er^{3+}-doped bismuth-tungsten-tellurite glasses containing silver NPs and heat-treated for 1, 24, 48 and 72 h. The maximum enhancement in upconversion luminescence were observed for sample with 24 h of heat-treatments, due to presence of NPs with average size of 35 nm. There was no plasmon peak reported in this study, however, they conclude that a tail on the absorption spectrum in the blue region belongs to SPR which is not clearly observable due to small amount of silver NPs.

Amjad et al. prepared the Er^{3+}-doped magnesium phosphate [133, 134] and magnesium-tellurite [135] glasses embedding silver NPs. Introduction of silver NPs with average size of 37 nm enhanced the upconversion intensities of Er^{3+} ions under 797 nm excitation wavelength by a factor of 2.04 and 1.99 for 540 and 634 nm emission bands, respectively. SPR band of Ag NPs was observed in an Er^{3+}-free phosphate glass to be centered at 528 nm [133]. The enhancement is mainly attributed to enhanced local field and partly discussed in terms of ET from Ag NPs to Er^{3+} ions. HR-TEM imaging revealed the cubic closed pack structure of the silver NPs as the lattice constant were measured to be 2.13 Å which is attributed to d_{200} crystallography characterize of silver ($d_{200} = 2.05$Å, JCPDS No.030931).

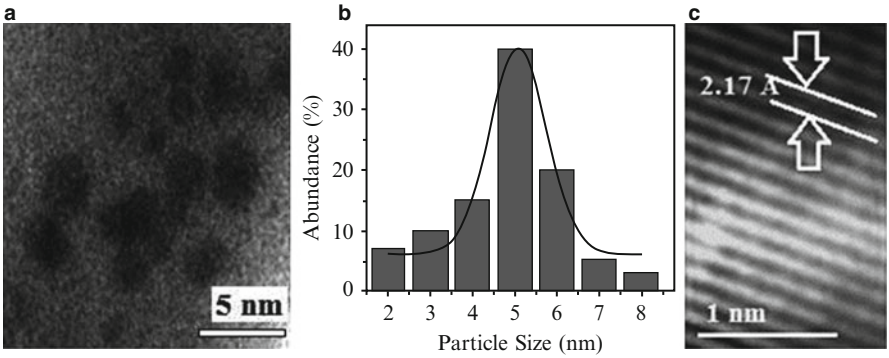

Fig. 14.8 (**a**) TEM, (**b**) size abundance, and (**c**) HR-TEM microscopic images of silver NPs embedded phosphate glass having average size of about 5 nm and grown along (200) crystallographic plane (Micrograph is taken from [134])

The effect of heat-treatment on Ag NPs-Er^{3+}-co-doped phosphate glass is also investigated [134]. The enhancement in visible bands up to 2.2 times was reported due to annealing the glasses up to 40 h at 300 °C. Comparing to their previous report [133], the plasmon peak shows a blue-shift (observed at 488 nm) and the size of NPs are clearly smaller, about 5 nm in average. However, HR-TEM image confirms the presence of Ag NPs with $d_{200} = 2.17$ Å. In the case of Er^{3+}-doped magnesium tellurite glasses, the addition of 0.5 mol% Ag NPs resulted in more efficient enhances in upconversion emission up to 3.33 times for the red emission after 24 h of annealing [135]. The silver NPs with average size of 12 nm were observed with SPR band located at ~534 nm. However, it is reported in their work that luminescence intensities in whole visible range quenched due to over-heat-treatments. The ET from Er^{3+} ions to Ag NPs and reabsorption by SPR were mentioned as main explanations for such quenches (Fig. 14.8).

The effect of silver NPs on the optical and structural properties of Er^{3+}-doped zinc tellurite glass is investigated by Dousti et al. [96, 106, 136]. The absorption bands of Er^{3+} ions are located at 445, 488, 522, 654, 800, 976 and 1526 nm and ascribed to the electric transitions from the $^4I_{15/2}$ ground state to $^4F_{3/2}$/$^4F_{5/2}$, $^4F_{7/2}$, $^2H_{11/2}$, $^4F_{9/2}$, $^4I_{9/2}$, $^4I_{11/2}$ and $^4I_{13/2}$ excited states, respectively. The introduction of Ag NPs enhanced the upconversion emissions of green and red bands centered at 520, 550 and 640 nm by 4–6 times. The enhancement is attributed to the presence of silver NPs with average size ~10 nm and with SPR localized at 522 nm. By introduction of 0.5 mol% of Ag NPs with an average size of 12 nm, 3.5-fold enhancement was observed for green emission ($^2H_{11/2} \rightarrow {}^4I_{15/2}$) due to formation and growth of NPs after 8 h of annealing (Fig. 14.9) [136]. After 2 h annealing, two peaks in UV-Vis-IR spectra were attributed to SPR, centered at 550 and 580 nm. After 8 h annealing, they observed three SPR peaks which are ascribed to different modes of oscillating particles. In the case of 1 mol% of Ag NPs in the same glassy system, enhances up to 6.5 folds were observed for upconversion emissions after 4 h annealing at temperatures above the T_g. Average size of manipulated Ag NPs

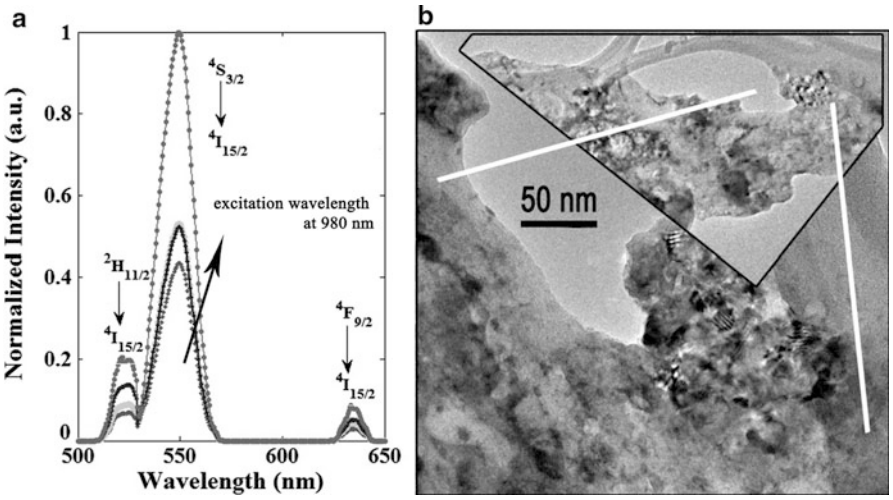

Fig. 14.9 (**a**) Upconversion emission of Er^{3+}-doped tellurite glasses is enhanced in presence of silver nanoparticles and heat-treatment up to 20 h (Adopted from [104]) (**b**) TEM image of silver nanoparticles with average size of about 12 nm which are formed by heat-treatment up to 8 h (Micrograph is taken from [136])

were 14 nm, with two SPR bands at 560 and 594 nm, an indicative of formation of non-spherical NPs.

Qi et al. [137] showed that presence of silver NPs enhances the 1.53 μm emission of Er^{3+}-doped TeO_2-Bi_2O-TiO_2 glasses under 980 nm LED excitation. SPR band is observed at 537 nm and size of NPs was found to be ~13 nm. Er^{3+}-doped lead-tellurite glass containing silver ions (using Ag_2O) and silver nanoparticles (using AgNPs) are also studied by Culea et al. [138]. The structural and optical properties of these sets of glasses are investigated using different techniques. However, there is no evidence of existence of Ag NPs using XRD, UV-Vis absorption and photoluminescence spectroscopic techniques.

The influence of gold NPs on the upconversion emission and Judd-Ofelt parameters of Er^{3+}-doped tellurite glass is investigated by Awang et al. [139, 140] and Sazali et al. [141]. However, the correlation of upconversion and Judd-Ofelt parameters is still not clearly understood. Refractive index, density, the quality factor, and thermal stability of this glassy system are also increased by addition of Au content. Upon heat-treatments at various temperatures, the glasses showed further enhancements of upconversion luminescence due to formation of non-spherical Au NPs [142]. The effect of the heat-treatment duration on the same glass shows improvement of green emission [143]. Surface plasmon band of silver NPs in the bismuth glass is observed at 555 nm [144]. In this glass, the infrared emission of Er^{3+} ions centered at 1554 nm experienced an enhancement in the order of 7.2 times due to local filed enhancement by SPR. Judd-Ofelt intensities parameters of these glasses are also increased by addition of Ag NPs. The enhancement of upconversion luminescence of Er^{3+} ions in zinc boro-tellurite glass is also

reported [145]. Surface plasmon band is observed at 630 nm for silver NPs with average size of 4.5 nm as captured by TEM imaging for 0.1 mol% of silver NPs doped tellurite glass. In another study, the luminescence of Er^{3+} ions enhanced by 4 times due to introduction of silver NPs which are embedded through an heat-treatment of borate glass, where SPR band is observed at 410 nm [146]. They showed that extra heat-treatments results in decrease of the size of NPs, as observed by a blue-shift (380 ← 410 nm) in SPR band of Ag NPs.

Similar to above-mentioned reports, the effect of noble metallic NPs on the optical properties of Er^{3+}-doped in various glasses are investigated wide and large [147–150]. The effect of gold and silver NPs on the upconversion emissions of Er^{3+}/Yb^{3+} co-doped glasses are also reported by different authors, and evident enhancements are observed [151–154].

14.4.3 Nd^{3+}-Doped

Nd^{3+}-doped antimony glass embedding $gold_{core}@silver_{shell}$ NPs are studied by different spectroscopic techniques [155]. XRD and SAED showed the formation of core-shell NPs by diffraction patterns along the (111) and (200) crystal planes. TEM imaging confirmed the presence of NPs by average size of about 22–107 nm. The plasmon peaks of NPs are observed by UV-Vis-IR absorption spectroscopy in the range of 532–675 nm, which showed a red-shift by increasing the concentration of $gold_{core}$ NPs. Five-fold intensity enhancement of upconversion emissions of Nd^{3+} ion is observed under 805 nm excitation wavelength. The enhancements of two-major bands centered at 540 nm ($^4G_{7/2} \rightarrow {}^4I_{9/2}$; green) and 649 nm ($^4G_{7/2} \rightarrow {}^4I_{13/2}$; deep-red) are attributed to local field effect induced by plasmonic core-shell metallic NPs.

Frequency upconversion emissions in Nd^{3+}-doped lead-germanate glass containing silver NPs are enhanced under 805 nm excitation wavelength [156]. The absorption band of silver NPs are not observed due to the low concentration of this specie, however, TEM showed the nanoparticles with varying size from 2 to 50 nm. Enhancement of upconversion emissions of Nd^{3+}-doped lead-tellurite glass under 800 nm excitation wavelength is also reported by Dousti [157]. Sixteen-fold enhancement is attributed to large local field in vicinity of silver NPs having an average size of 18 nm. Different interactions and growth process is also described and silver crystalline peaks are observed in XRD patterns of glassy system at $2\theta = 44^\circ$ (Fig. 14.10).

14.4.4 Sm^{3+}-Doped

The effect of noble metallic NPs in antimony glass and glass-ceramic containing Sm^{3+} ions were reported by Som and Karmakar [155, 158–160], and enhanced

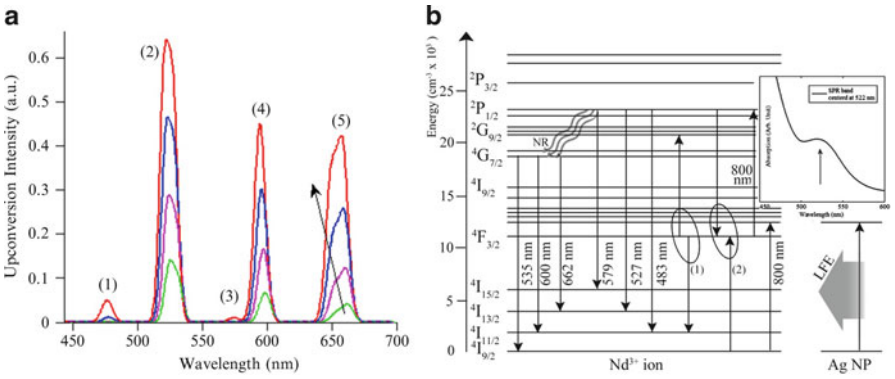

Fig. 14.10 (**a**) Enhancement in upconversion emission of Nd^{3+}-doped tellurite glass by increasing the concentration of silver nanoparticles from 0 to 0.1, 0.5 and 1 mol%. (**b**) SPR band of silver NPs in tellurite glass is centered at 522 nm [157]

luminescence in samarium emissions were observed. The red upconversion luminescence (centered at 636 nm) of Sm^{3+} ions is studied in presence of core-shell bimetallic nanoparticles (Au-Ag NPs) in an antimony glass system. Two-fold enhancement is observed under the excitation at 949 nm and the surface plasmon band is observed in the range of 554–681 nm for various concentrations of metal [102]. Similar results are observed by addition of silver NPs in Sm^{3+}-doped silicate glass, where Ag ions are reduced to Ag neutral particles by antimony oxide as the oxidant agent [161].

Li et al. [162] also investigated the effect of silver NPs on optical properties of Sm^{3+}-doped silicate glasses. Different silver species are formed in the silicate glass by an Ag^{+}-Na^{+} ion exchange process. Although enhancement of luminescence under 270/250 and 355 nm is observed due to energy transfer from Ag^{+} and Ag^{+}-Ag^{+} to Sm^{3+} ions, respectively, the presence of NPs quenches the luminescence under 401 excitation wavelength. They concluded that the competitive absorptions by Sm^{3+} ions and Ag NPs (SPR ~ 420 nm) suppress the luminescence of Sm^{3+} ions.

Jimenez and Sendova [163] studied the effect of silver species (Ag NPs and non-plasmonic clusters) on the luminescence intensity of Sm^{3+}-doped aluminophosphate glass as a function of holding heat-treatment time. The SPR band is not observed up to 50 min of heat-treatments, however the luminescence enhances gradually. The SPR band emerges and intensifies by further heat-treatments up to 120 min, while the luminescence intensity of Sm^{3+} ions quenches progressively. They concluded that the enhancements and quench in the luminescence are associated to the presence of non-plasmonic clusters and NPs, respectively.

In a recent study, the effect of the heat-treatment on the upconversion luminescence of Sm^{3+}-doped borosilicate glasses containing silver NPs are examined [161]. The silver ions are reduced by Sb^{3+} ions as oxidation agents and NPs are grown gradually by increasing the time of heat-treatments up to 20 h. It is stated that

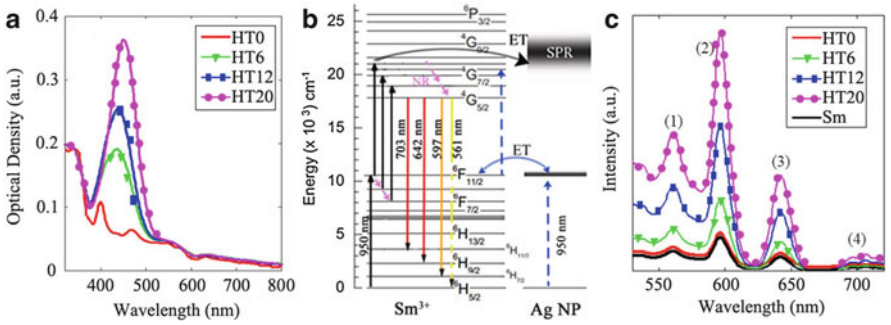

Fig. 14.11 (**a**) UV-Vis-NIR absorption spectra of Sm^{3+}-AgNPs doped borosilicate glass without (HT0) and after 6 (HT6), 12(HT12) and 20 h (HT20) heat-treatments. (**b**) Schematic partial energy level diagram of Sm^{3+} ion in vicinity of silver NP where two-photon absorption mechanism results in upconversion emission of this ion. Probable energy transfer (ET) and nonradiative (NR) decay mechanisms are also illustrated. (**c**) Emission spectra of Sm^{3+}-doped glasses without (Sm) and after incorporation of Ag NPs (Data are adopted from [161])

the further heat-treatments result in a translucent glassy component which is not favorable for optical applications. The surface plasmon band of silver NPs in this glass is observed at ~436 nm which red-shifts to 450 nm by increasing the heat-treatments, indicative of a growth in the size of NPs from 8 to 14 nm (Fig. 14.11).

The effect of annealing temperature on the surface plasmon band position of silver NPs embed in Sm^{3+}-doped lithium borate and sodium borate glasses are also investigated [164]. The SPR band shows a disordered shift in the range of 425–445 nm with varying the annealing temperature from 430 to 510 °C. However, the plasmonic effect of silver is too diminutive and causes a small improvement of emissions from Sm^{3+} ions.

The enhancement in the luminescence of Sm^{3+}-doped tellurite glass by introduction of silver NPs is also given in Ref. [165]. The author showed that under 406 nm excitation wavelength, the emission line at 645 nm enhances up to 130 % by addition of concentration of Ag NPs up to 1 mol%. The increased luminescence of the Sm^{3+} ions are attributed to localized surface plasmon resonance of silver NPs.

The effect of the silver NPs on the Sm^{3+}-doped different media are also available. For instance, Kaur et al. [166] reported on the enhanced luminescence of Sm-complex (PVA) where the Ag NPs were formed by laser irradiation at 355 nm. The SPR band is observed around 402–405 nm and emissions in the visible range are enhanced for both 355 and 400 nm excitation wavelengths. The lifetime of 595 nm emission of Sm^{3+} ions under 355 nm is increased in presence of Ag NPs. Although, there are not many reports on the effect of noble metallic NPs on the Sm^{3+}-doped glasses and glass-ceramics, different authors contributed to study the influence of other NPs (such as CdS NPs) on the luminescence of Sm^{3+} ions doped glasses [167].

14.4.5 Dy^{3+}-Doped

The influence of Ag NPs on the luminescence decay of Dy^{3+}-doped aluminophosphate is reported by Jimenez [168]. Although the incorporation of metallic NPs in this system quenched the luminescence of Dy^{3+} ions under 450 nm excitation wavelength, the new concept of "plasmonic diluents" highlighted this work as a worthy publication to think over. The mechanism behind the plasmonic diluents is similar to lowering the effective concentrations of ions, where lower absorptions takes place in the system. On the other word, the resonance excitation of the system results in an energy transfer from ion to particle (silver NPs) which is a detrimental factor for subsequent PL processes, and results in luminescence quenching. Moreover, Jimenez showed that the increasing the volume fraction of the silver NPs by increasing the heat-treatment durations, prolongs the fast and slow decay times of Dy^{3+} ions.

On the other hand, in another study, the upconversion emissions of Dy^{3+}-doped tellurite glasses are enhanced by heat-treated silver NPs [169]. Four-time enhancement is observed for visible emissions under 800 nm excitation wavelength. Silver NPs having an average size of 18 nm are observed and the enhancement in photoluminescence feature is described as the modification of local field due to difference between dielectric constant of medium and metallic particle (Fig. 14.12).

There are not many reports on the influence of noble metallic NPs on the optical properties of Dy^{3+}-doped glasses or glass-ceramics. However, the influence of Cu NPs on the luminescence of Dy^{3+}-doped barium-phosphate glasses is studied [170]. Cu^{2+} and Cu^{+} ions are reduced to Cu^{0} NPs as $Cu^{2+} + Sn^{2+} \rightarrow Cu^{0} + Sn^{4+}$ and $2Cu^{+} + Sn^{2+} \rightarrow 2Cu^{0} + Sn^{4+}$, respectively. The glasses are annealed for 30, 60 and 120 min, but all the observed photoluminescence emissions are quenched under 350 and 450 nm excitation wavelength. The quench is attributed to nonradiative loss of excitation energy in Dy^{3+} ions with an energy transfer from ion to NP. The effect of gold is also reported on the optical properties of Dy^{3+}- and Eu^{3+}-doped silica nanoparticles [171].

14.4.6 Tm^{3+}-Doped

Assumpcao et al. [172] studied the upconversion emission of Tm^{3+}-doped zinc tellurite glasses containing silver NPs. In the latter work, they investigated the infrared-to-visible and infrared-to-infrared upconversion process under 1050 nm excitation wavelength and the observed enhancements of luminescence is attributed to the increased local field by silver NPs after heat-treatments. Assumpcao et al. [173] also studied the frequency upconversion emissions from Tm^{3+}-Yb^{3+} co-doped germanate glasses embedding silver NPs. They showed that infrared (980 nm)-to-visible (480 nm) upconversion emission in the current system is due to the energy transfer from Yb^{3+} ions to Tm^{3+} ions. They concluded that the

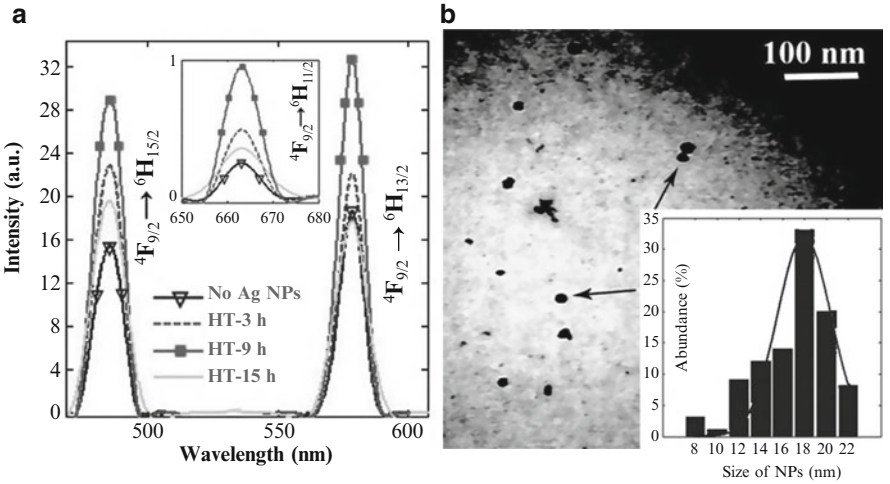

Fig. 14.12 (**a**) Upconversion emissions of Dy^{3+}-doped tellurite glasses are enhanced and quenched after 9 and 15 h of heat-treatments (HT), respectively, under 800 nm excitation wavelength. (**b**) TEM image of silver NPs embedded tellurite glass after 9 h heat-treatments with an average size of about 18 nm [169]

absorption of two, three, and four photons result in upconversion emissions at 800, 652–477 and 542 and 455 nm, respectively. Presence of silver NPs is confirmed by TEM technique and NPs with average size of about 10 nm (isolated) and 80 nm (aggregated) are captured. Intensity of the upconversion emissions at vicinity of SPR band are enhanced up to 30 %. Moreover, Assumpcao et al. [174] showed that the SPR band for this glassy system can be observed by annealing the samples at higher temperature ($T > 480$ °C) for 6 h. As reported, the intensity of SPR absorption band and upconversion emissions increases by increasing the heat-treatment temperature up to 540 °C.

The influence of silver NPs on upconversion emission of Tm^{3+}-Yb^{3+} co-doped zinc tellurite glass is also reported [175]. However, there is no SPR band observed for this glass system up to 72 h of heat-treatment at 325 °C. Upconversion emissions in this system are associated to the energy transfer from Yb^{3+} ions to Tm^{3+} ions, with only 2 and 3-photons absorption mechanism for bands at infrared and visible regions, respectively. Silver NPs enhances the upconversion emissions in order of 300 % under 980 nm excitation wavelength. Kassab et al. [176] reported that the large Judd-Ofelt intensity parameters of Tm^{3+} ions ($\Omega_2 = 15.65 \times 10^{-20}$ cm^2) in $Tm^{3+}-Yb^{3+}$-co-doped zinc-tellurite glass containing silver NPs can nominate them as optically stimulated quantum electronic devices and optically operated fibers.

Singly Tm^{3+}-doped PbO-GeO_2 oxide glasses containing silver NPs are also investigated by the latter group [177]. Upconversion emissions are enhanced in presence of silver NPs under 1050 excitation wavelength for heat-treatment up to 24 h. Further heat-treatments (up to 72 h) resulted in a quenching in luminescence

spectra. Moreover, they concluded that the continuous heat-treatments stimulate the NPs to aggregate while non-continues heat-treatments with a step of 12 h prevents the aggregation of NPs. In another study, Qi et al. [178] observed significant enhancement in emissions of Tm^{3+} ions due to participation of Ag NPs in the bismuth germanate glasses.

Triply doped Tm^{3+}-Er^{3+}-Yb^{3+} lead germanate oxide glasses containing silver NPs is also investigated [179]. The SPR band is observed at 400–500 nm region and the broad FWHM of this band is attributed to presence of NPs with different sizes and shapes. For excitation at 980 nm, enhancements of about 60 % are observed for five emission bands. Two bands are associated to Tm^{3+} ions which are centered at 477 and 652 nm, and three bands located at 530, 550 and 660 nm are originated form Er^{3+} ions. Energy transfers among these species are discussed in latter reference. Figure 14.13 shows a schematic partials energy level diagram of this tri-doped glass. The same doping system embedded in a tellurite glass containing silver NPs is also reported by the same group [180] where efficient mid-infrared emissions from Er^{3+} (1.55 μm) and Tm^{3+} ions (1.86 μm) are observed. Moreover, efficient energy transfer from Yb^{3+} ions to Er^{3+} and Tm^{3+} ions are concluded by time-resolved luminescence investigations. The decay lifetime of $^4F_3 \rightarrow {}^3H_6$ (Tm^{3+}) shortened from 3.4 to 2.9 ms by addition of silver NPs and lifetime of $^4I_{13/2} \rightarrow {}^4I_{15/2}$ (Er^{3+}) decreased from 2.4 to 1.7 ms. $Tm^{3+}/Yb^{3+}/Er^{3+}$ tri-doped oxyfluorogermanate glasses containing silver NPs are also reported [181]. The authors showed that the introduction of silver NPs reduces the glass thermal stability as well as glass transition and crystallization temperatures. A broad absorption band around 400–500 nm is attributed to surface plasmon band of silver which is extended up to 800 nm for further annealing time intervals. Silver NPs are grown from 4 to 10 nm by increasing the annealing time from 34 to 51 h. The intensity of all the observed upconversion emissions (emissions at 476, 524, 546 and 658 nm, and excitation at 980 nm) increases by increasing the annealing time up to 34 h, while it quenches for further heat-treatments. All the emissions originate from a two-photon absorption process. The effect of Ag_2O concentration on the upconversion emission of the $Tm^{3+}/Yb^{3+}/Er^{3+}$ doped oxyfluorogermanate glasses is also studied by the same research group [13]. They showed that by increasing the molar concentration of Ag_2O up to 1.5 mol%, the upconversion luminescence of both Tm^{3+} and Er^{3+} ions increases, whereas further introduction of Ag NPs result in the quenching of emissions. The presence of non-spherical NPs in this study is emerged by appearance of two SPR bands; transverse and longitudinal modes located at 344 and 425 nm, respectively.

14.4.7 Tb^{3+}-Doped

A photoluminescence enhancement of about 1.6 times is observed in Tb^{3+}-doped silicate glass due to incorporation of silver NPs [182]. Under excitation at 488 nm, the emissions of Tb^{3+} ions at visible region (537, 578 and 612 nm) are enhanced

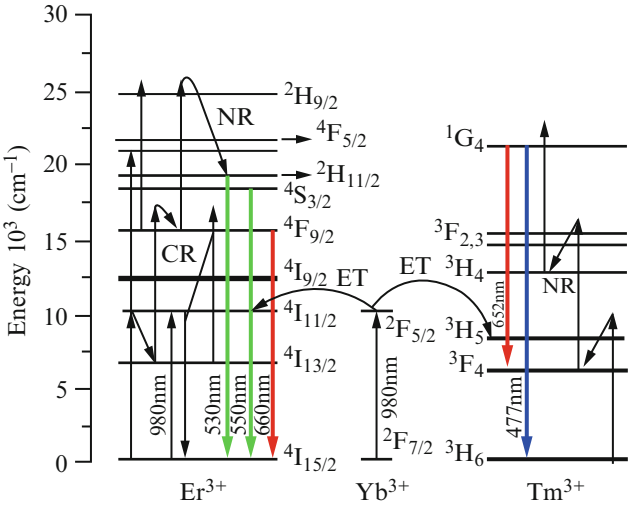

Fig. 14.13 Schematic partial energy level diagram of Tm^{3+}-Er^{3+}-Yb^{3+}tri-doped glasses showing upconversion emissions, energy transfer (ET), cross-relaxation (CR) mechanisms and nonradiative decays (NR) (Adapted from [179])

thanks to the increased local field by metallic silver NPs. Tb^{3+}-doped silicate glass containing silver NPs are also investigated by Piasecki et al [183, 184]. SPR band is observed at 480 nm and the luminescence lines are enhanced under 325 nm excitation wavlenegth. Maximum enhancement of 1.8 times is obtained for sample containing 0.5 mol% of silver after 3 h of heat-treatments.

The SPR band of silver NPs embedded Tb^{3+}-doped silicate glass is located at 420 nm and its intensity increases by increasing the concentration of silver NPs [185]. The emissions of Tb^{3+} ions in the range of 400–700 nm are enhanced for the sample containing 3 mol% of $AgNO_3$ and quenched in the glass sample embedding 5 mol% of silver NPs. The enhancement of about 35 % in emission intensity of Tb^{3+} ions (543 nm) in a silica system is also observed as the lifetime of this fluorescence reduces. Such fluorescence enhancement and increased radiative decay rates are attributed to the increased local filed induced by silver NPs [186].

Verma et al. [187] investigated the effect of silver NPs on the fluorescence of Tb^{3+}-doped aluminosilicate glass. Silver NPs are prepared by laser ablation in distilled water, and embedded in the glass following a sol-gel technique. Surface plasmon resonance band of silver is observed at 404 nm, and their radius is estimated to be ~6.48 nm by measuring the FWHM of SPR band. The lifetime of the $^5D_4$ level of terbium is increased from 310 to 420 μs in the presence of silver NPs. The emission intensity of rare earth ions enhances up to 100 % which is a result of the energy transfer from the excited silver NPs to Tb^{3+} ions.

Sodium-lead-zinc-tellurite glass doped with Tb^{3+}/Eu^{3+} ions and silver NPs showed a plasmon peak centered at 490 nm after a long heat-treatment [188]. The large enhancement in luminescence of Eu^{3+} ions (centered at 590 and 614 nm) is

attributed to simultaneous contributions of (i) energy transfer among Eu^{3+}-Tb^{3+} ions and (ii) intensified local field in vicinity of Ag NPs and Eu^{3+} ions. They observed that the integrated emission of Eu^{3+} ions increases by increasing the annealing time of sample up to 62 h.

In addition, Tb^{3+}-Yb^{3+} doped aluminosilicate glasses containing silver NPs are investigated by Pan et al. [189]. The SPR peak is observed at 420 nm which shows no shift by further annealing. However, the presence of silver NPs with size of about 3–7 nm is confirmed by TEM. Upconversion luminescence of Tb^{3+} ions is enhanced after 5 h of heat-treatments, but longer treatments quenched the intensity of PL spectrum. Moreover, the normal luminescence under 488 nm excitation wavelength is quenched due to the quantum cutting effect.

14.4.8 Pr^{3+}-Doped

Kassab et al. [94] reported that the luminescence characteristics of Pr^{3+} in lead-tellurite glass enhances due to presence of silver NPs with average size around 3.5 nm, which are formed by annealing at 350 °C for 7 h. Rai et al. also studied the influence of silver NPs on the optical properties of Pr^{3+}-doped zinc-tellurite glasses [190]. Upconversion emission of Pr^{3+} ions centered at ~482 and ~692 nm are observed under the excitation with a nanosecond laser operating at 590 nm. An enhancement of about 120 % is achieved for the integrated intensities of those emissions after heat-treating the sample containing silver NPs up to 40 h. Enhancement in luminescence of Pr^{3+}-doped PbO-GeO_2 glasses are also observed in presence of isolated silver particles and aggregated silver NPs with an average diameter of 2 nm and less than 100 nm, respectively [191]. They showed that the amplitude of surface plasmon band of silver NPs is centered at 464 nm in this glass and increases by increasing the heat-treatment durations. Both energy transfer mechanism from nanoparticle to ion and modified local filed around the Pr^{3+} ions are discussed as the factors of enhancement, however the exact contribution of each phenomenon was not concluded. Enhancement in emissions from Pr^{3+} ions doped zinc-tellurite glass containing silver NPs is also reported [192]. The influence of large local field on the Pr^{3+} ions is discussed as the major factor for enhancements of visible emission under both 470 nm (Stokes) and 586 (anti-Stokes) excitation wavelengths.

Furthermore, the effect of silver NPs on the luminescence of Pr^{3+}-doped borate glass is investigated [117]. Both excitation and luminescence spectra showed enhancement in the emission line centered at 558 nm and excitation at 442 nm, respectively. The increased intensity of luminescence is attributed to "the resonance between the energy band with the levels of the Pr^{3+} ions". As mentioned before (see 4.1), the formation of silver NPs in this system is slower than its counterpart Eu^{3+}-doped glass, and the size of NPs are 4 times large in the case of Eu^{3+}-doped samples.

14.4.9 Ho^{3+}-Doped

The enhancement in the upconversion emissions of Ho^{3+}/Yb^{3+} co-doped tellurite glass is also observed [193] by incorporation of silver NPs which are formed by addition of $AgNO_3$ to the glassy host, melted at 900 °C for 30 min and annealed above its glass transition temperature. Silver NPs with average diameter size of about 3–12 nm show a SPR absorption band centered at 560 nm and contribute to ~2.5 times enhancement in intensity of emissions at 546 and 657 nm under 980 nm excitation wavelength.

Although there are not many reports on the effect of noble metallic NPs on the luminescence of Ho^{3+}-doped glasses, some research group investigated the effect of nanocrystals on such systems. For instance, Zhang et al. [194] reported on the enhanced 2.0 μm emission of Ho^{3+}-Tm^{3+}-co-doped glass ceramics containing BaF_2 nanocrystals. Efficient energy transfer from Tm^{3+} to Ho^{3+} ions is attributed to low phonon energy environment and reduced ionic distance of lanthanide species after incorporation into nanocrystal embedding glass ceramics.

14.5 Summary

Improving the optical and thermal properties of glasses, glass-ceramics and crystals is of supreme importance in order to develop the smart optical devices, such as solid state lasers, amplifiers, undersea cameras, telecommunication devices, color displays and so on. The aim of this chapter was to revisit the current achievements on the state of art in understanding the role of metallic NPs on the optical properties of some rare earth-doped oxide glasses. Until now, various studies have been done to enhance the properties of glasses containing RE ions. Incorporation of larger concentrations of RE ions, introduction of second dopant, thermal treatments, different synthesizing methods and varying the glass host matrix are among the common techniques in order to modify the environment of the RE ions, which significantly can alter its optical properties. Room temperature optical properties of RE-doped glasses containing metallic NPs synthesized by a melt quench technique have been studied by many researchers. Analytical techniques such as UV-Vis absorption and photoluminescence spectroscopy have been used to optically characterize the glasses and the data showed that Stokes and anti-Stokes luminescence of most of the proposed glassy systems has improved by addition of metallic NPs.

In this chapter, initially, a short introduction on the importance of material science, glass and glass-ceramic technology was explained in the first section. It was followed by a chronological study on the history of glasses during the last centuries. This section was continued by a review on spectroscopic properties of rare earth ions in materials in general and glasses in particular. The developed theories and models on optical properties of rare earth ions and interactions between light and ions and ion-ion interactions were explained. The energy level diagram of

electronic configuration of rare earth ions and probable mechanisms, such as energy transfer and relaxation processes were summarized. Section 14.3 was devoted to study the interaction of light with metallic NPs in the dielectric media. The effect of shape and size of NPs on the optical behavior of the system are given. The custom methods to prepare and observe the NPs and widespread applications of plasmonic phenomenon were asserted. Finally, recent results on the influence of metallic NPs on the glasses containing RE ions are listed in Sect. 14.4. Based on the results, the potentiality and applicability of these studies are concluded in current section and the new achievements and importance of the research is ascertained. However, there are many characteristic analyses which are not provided in the literature. Different preparation methods and environmental situations may alter the functionality and potentiality of the samples and several suggestions are listed for further research as follows:

(i). Structural properties of the studied glass samples can further be investigated through Raman spectroscopy, NMR, and ESR.
(ii). Thermal properties can be analyzed to correlate the nucleation of NPs with thermal characteristics of glasses, especially at the heat-treatment temperatures.
(iii). Trivalent rare earth ion possesses various excited states. The optical investigation while doped with different co-dopants can be interesting where the system can provide white-light emissions through the second and third non-linear processes, and energy transfers.
(iv). Various preparation techniques are suggested by different authors to synthesize a glass. The usage of different melting and annealing temperature, and pouring in different environments may also modify the structural and consequently the thermal and optical properties of glasses.
(v). Ceramics show completely different structural, thermal and optical properties with respect to amorphous glass system. Therefore, the preparation of ceramics and glass-ceramics with the same compositions can be also recommended to observe the behavior of a noble system. One may arise for preparation of thin films by same composition.

As the final point, it is of utmost importance to recall that the controlling the size and shape of the NPs is an imperative factor to establish an optically favorable glassy system with enhanced optical properties. As revealed in this chapter, the incorporation of metallic NPs can enhance the optical properties of the RE-doped oxide glasses. Therefore, further investigations are suggested to provide a suitable glassy system and to correlate the controlling parameters with size, shape and performance of the NPs in such optical materials.

Acknowledgments The experimental data given in this work has been collected by the authors during their doctoral degree and later while working as a post-doctoral fellowship or a professorship. The authors would like to thanks many people who has contributed in discussing the results, providing funds and grants, giving feedbacks and commenting on the work to improve it in both terms of scientific and publication subjects. Especial thanks to Prof. Dr. Md. Rahim Sahar for his

supports, and to Prof. Dr. Andrea de Camargo for her valuable comments. Moreover, last but not least, we would like to acknowledge the kind invitation form Prof. Chris. D. Geddes for giving us such a great opportunity to contribute in this Book.

References

1. Zanotto ED (2010) A bright future for glass-ceramics. Am Ceram Soc Bull 89:19–27
2. Tait H (ed) (1991) Five thousand years of glass. The British Museum Press, London
3. Plodinec MJ (2000) Borosilicate glasses for nuclear waste immobilisation. Glass Technol 41:186–192
4. Brian Starling L, Stephan JE (2002) Calcium phosphate microcarriers and microspheres. US Patent 6210715 B1, 6,358,532 B2
5. Clinton JM, Coffeen WW (1984) Low melting glasses in the system B_2O_3-ZnO-CaO-P_2O_5. Am Ceram Soc Bull 63:1401–1404
6. Daimer J, Paschke H (1990) Glass sealant containing lead borate glass and fillers of mullite and cordierite. US Patent 5145803 A, 5,145,803
7. Koudelka L, Mošner P (2001) Study of the structure and properties of Pb–Zn borophosphate glasses. J Non Cryst Solids 293–295:635–641
8. Stokowski SE, Saroyan RA, Weber MJ (1981) Nd-doped laser glass spectroscopic and physical properties. Lawrence Livermore National Laboratory, University of California, Livermore
9. Stocker HJ (1969) Bulk and thin film switching and memory effects in semiconducting chalcogenide glasses. Appl Phys Lett 15:55
10. Poulain M (1983) Halide glasses. J Non Cryst Solids 56:1–14
11. Baldwin CM, Almeida RM, Mackenzie JD (1981) Halide glasses. J Non Cryst Solids 43:309–344
12. El-mallawany RAH (2002) Tellurite glasses handbook: physical properties and data. CRC Press, Boca Raton
13. Hu Y, Qiu J, Song Z, Zhou D (2014) Ag_2O dependent up-conversion luminescence properties in Tm^{3+}/Er^{3+}/Yb^{3+} Co-doped oxyfluorogermanate glasses. J Appl Phys 115:083512
14. www.scopus.com. Accessed 15 July 2014
15. Mauro JC, Zanotto ED (2014) Two centuries of glass research: historical trends, current status, and grand challenges for the future. Int J Appl Glass Sci 15:313–327
16. Thiel CW, Sun Y, Cone RL (2002) Photonic materials and devices progress in relating rare-earth Ion 4f and 5d energy levels to host bands in optical materials for hole burning, quantum information and phosphors. J Mod Opt 49:2399–2411
17. Jha A, Richards B, Jose G, Teddy-Fernandez T, Joshi P, Jiang X, Lousteau J (2012) Rare-earth Ion doped TeO_2 and GeO_2 glasses as laser materials. Prog Mater Sci 57:1426–1491
18. Pan Z, Sekar G, Akrobetu R, Mu R, Morgan SH (2012) Visible to near-infrared down-conversion luminescence in Tb^{3+} and Yb^{3+} Co-doped lithium–lanthanum–aluminosilicate oxyfluoride glass and glass-ceramics. J Non Cryst Solids 358:1814–1817
19. Dai S, Yu C, Zhou G, Zhang J, Wang G, Hu L (2006) Concentration quenching in erbium-doped tellurite glasses. J Lumin 117:39–45
20. Pokhrel M, Kumar GA, Balaji S, Debnath R, Sardar DK (2012) Optical characterization of Er^{3+} and Yb^{3+} Co-doped barium fluorotellurite glass. J Lumin 132:1910–1916
21. Malta OL, Santa-Cruz PA, De Sá GF, Auzel F (1985) Fluorescence enhancement induced by the presence of small silver particles in Eu^{3+} doped materials. J Lumin 33:261–272
22. De Araújo CB, Oliveira TR, Falcão-Filho EL, Silva DM, Kassab LRP (2013) Nonlinear optical properties of PbO–GeO_2 films containing gold nanoparticles. J Lumin 133:180–183
23. Hufner S (1978) Optical spectra of rare earth compounds. Academic, New York

24. Becker PC, Olsson NA, Simpson JR (1999) Erbium-doped fiber amplifiers. Academic, San Diego
25. Maheshvaran K, Marimuthu K (2012) Concentration dependent Eu^{3+} doped boro-tellurite glasses – structural and optical investigations. J Lumin 132:2259–2267
26. Zheng H, Gao D, Fu Z, Wang E, Lei Y, Tuan Y, Cui M (2011) Fluorescence enhancement of Ln^{3+} doped nanoparticles. J Lumin 131:423–428
27. Judd BR (1962) Optical absorption intensities of rare-earth ions. Phys Rev 127:750–761
28. Ofelt GS (1962) Intensities of crystal spectra of rare-earth ions. J Chem Phys 37:511–520
29. Walsh BM (2006) Judd-Ofelt theory: principles and practices. In: Di Bartolo, Baldassare, Forte, Ottavio (eds) Advances in spectroscopy for lasers and sensing. Springer, Netherlands, pp 403–433
30. Carnall WT, Fields PR, Rajnak K, Ranjak K (1968) Electronic energy levels in the trivalent lanthanide aquo ions. I. Pr^{3+}, Nd^{3+}, Pm^{3+}, Sm^{3+}, Dy^{3+}, Ho^{3+}, Er^{3+}, and Tm^{3+}. J Chem Phys 49:4424
31. Weber MJ, Myers JD, Blackburn DH (1981) Optical properties of Nd $^{3+}$ in tellurite and phosphotellurite glasses. J Appl Phys 52:2944–2946
32. Rahman HU (1972) Optical intensities of trivalent erbium in various host lattices. J Phys C Solid State Phys 5:306–315
33. Yang J, Dai S, Dai N, Wen L, Hu L, Jiang Z (2004) Investigation on nonradiative decay of 4I13/2-4I15/2 transition of Er^{3+} -doped oxide glasses. J Lumin 106:9–14
34. Chen Y, Huang Y, Huang M, Chen R, Luo Z (2004) Spectroscopic properties of Er^{3+} ions in bismuth borate glasses. Opt Mater 25:271–278
35. Nandi P, Jose G (2006) Spectroscopic properties of Er^{3+} doped phospho-tellurite glasses. Phys B Condens Matter 381:66–72
36. Snitzer E (1961) Optical maser action of Nd^{3+} in a barium crown glass. Phys Rev Lett 7(12):444–446
37. Kao KC (1966) Dielectric-fibre surface waveguides for optical frequencies. Proc Inst Electr Eng London 113:1151
38. Sandoe JN, Sarkies PH, Parke S (1972) Variation of Er^{3+} cross-section for stimulated emission with glass composition. J Phys D Appl Phys 5:1788
39. Stone J, Burrus CA (1973) Neodymium-doped silica lasers in end-pumped fiber geometry. Appl Phys Lett 23:388–389
40. Svendsen SM (1997) First installation of WDM, optical ADM and optical in-line amplifiers on long-haul cable links in Norway. Telektronikk 3:115
41. Snitzer E (1973) Lasers and glass technology. Ceram Bull 52:516–525
42. Izumitani T, Toratani H, Kuroda H (1982) Radiative and nonradiative properties of neodimium doped silicate and phosphate glasses. J Non Cryst Solids 47:87–99
43. Wang JS, Vogel EM, Snitzer E (1994) Tellurite glass: a news candidate for fiber devices. Opt Mater 3:187–203
44. Li-Yan Z, Li-Li H (2003) Evaluation of broadband spectral properties of erbium-doped aluminium flourophosphate glass. Chin Phys Lett 20:1836–1837
45. Auzel F (1990) Upconversion processes in coupled Ion systems. J Lumin 45:341–345
46. Dexter DL (1953) A theory of sensitized luminescence in solids. J Chem Phys 21:836–851
47. Kaplyanskii AA, MacFarlane RM (eds) (1987) Spectroscopy of solids containing rare-earth ion. North-Holland, Amsterdam
48. Barber DJ, Freestone IC (1990) An investigation of the origin of the colour the Lycurgus Cup by analytical electron microscopy. Archaeometry 32:33–45
49. Faraday M (1857) The Bakerian lecture : experimental relations of gold (and other metals) to light. Philos Trans R Soc London 147:145–181
50. Binning G, Rohrer H, Gerber C, Weibel E (1982) Surface studies by scanning tunneling microscopy. Phys Rev Lett 49:57–61
51. Binnig G, Rohrer H (1982) Vakuum Tunnel Mikroskop. Helv Phys Acta 55:128

52. Knight WD, Clemenger K, de Heer WA, Saunders WA, Chou MY, Cohen ML (1984) Electronic shell structure and abundances of sodium clusters. Phys Rev Lett 52:2141–2143
53. Brigger I, Dubernet C, Couvreur P (2002) Nanoparticles in cancer therapy and diagnosis. Adv Drug Deliv Rev 54:631–651
54. Hirsch LR, Stafford RJ, Bankson JA, Sershen SR, Rivera B, Price RE, Hazle JD, Halas NJ, West JL (2003) Nanoshell-mediated near-infrared thermal therapy of tumors under magnetic resonance guidance. Proc Natl Aced Soc USA 100:13549–13554
55. Storhoff JJ, Mirkin CA (1999) Programmed materials synthesis with DNA. Chem Rev 99:1849–1862
56. Lee K-C, Lin S-J, Lin C-H, Tsai C-S, Lu Y-J (2008) Size effect of Ag nanoparticles on surface plasmon resonance. Surf Coat Technol 202:5339–5342
57. Schwartzberg AM, Grant CD, Buuren TV, Zhang JZ (2007) Reduction of $HAuCl_4$ by Na_2S revisited : the case for Au nanoparticle aggregates and against Au_2S/AuCore/shell particles. J Phys Chem 111:8892–8901
58. Gou L, Murphy CJ (2005) Fine-tuning the shape of gold nanorods. Chem Mater 17:3668–3672
59. Sun Y, Mayers B, Xia Y (2003) Transformation of silver nanospheres into nanobelts and triangular nanoplates through a thermal process. Nano Lett 3:675–679
60. Gonzalez AL, Noguez C (2007) Influence of morphology on the optical properties of metal nanoparticles. J Comput Theor Nanosci 4:231–238
61. Zhang JZ, Noguez C (2008) Plasmonic optical properties and applications of metal nanostructures. Plasmonics 3:127–150
62. Prasad P (2004) Nanophotonics. Wiley, Hoboken
63. Mie G (1908) Beitrage Zur Optik Truber Medien, Speziell Kolloidaler Metallosungen. Ann Phys 3:377–445
64. Wooten F (1972) Optical properties of solids. Academic, New York
65. Shanmukh S, Jones L, Driskell J, Zhao Y, Dluhy R, Tripp RA (2006) Rapid and sensitive detection of respiratory virus molecular signatures using a silver nanorod array SERS substrate. Nano Lett 6:2630–2636
66. Schwartzberg AM, Olson TY, Talley CE, Zhang JZ (2006) Synthesis, characterization, and tunable optical properties of hollow gold nanospheres. J Phys Chem B 110:19935–19944
67. Sun Y, Mayers BT, Xia Y (2002) Template-engaged replacement reaction: a one-step approach to the large-scale synthesis of metal nanostructures with hollow interiors. Nano Lett 2:481–485
68. Xu K, Heo J (2013) Luminescence enhancement of CdS quantum dots in glass by Ag^+ ion exchange. J Am Ceram Soc 96:1138–1142
69. Zoval JV, Stiger RM, Biernacki PR, Penner RM (1996) Electrochemical deposition of silver nanocrystallites on the atomically smooth graphite basal plane. J Phys Chem 100:837–844
70. Henglein A (1993) Chemical and optical properties of small metal particles in aqueous solution. Isr J Chem 33:77–88
71. Quinten M (2011) Optical properties of nanoparticle systems: mie and beyond. Wiley-VCH Verlag & Co. KGaA, Weinheim
72. Smoluchowski MV (1916) Drei Vorträge Über Diffusion, Brownsche Molekularbewegung Und Koagulation von Kolloidteilchen. Phys Z 17:557–599
73. Ostwald W (1900) On the supposed isomerism of red and yellow mercury oxide and the surface tension of solid substances. Z Phys Chem 34:495–503
74. Yu CH, Tam K, Tsang ESC (2009) Chemical methods for preparation of nanoparticles in solution. In: Blackman JA (ed) Handbook of metal physics, 1st edn. Elsevier, Oxford
75. Liu G, Xu S, Qian Y (2000) Nanofabrication of self-assembled monolayers using scanning probe lithography. Acc Chem Res 33:457–466
76. Wang ZL (ed) (2000) Characterization of nanophase materials. Wiley, New York

77. Wang ZL (2000) Transmission electron microscopy of shape-controlled nanocrystals and their assemblies. J Phys Chem B 104:1153–1175
78. Binning G, Quate CF, Gerber C (1986) Atomic force microscope. Phys Rev Lett 56:930–933
79. Fleischmann, M, Hendra PJ, McQuillan AJ (1974) Raman spectra of pyridine adsorbed at a silver electrode. Chem Phys Lett 26:163–166
80. Kneipp K, Wang Y, Kneipp H, Perelman LT, Itzakan I, Dasari RR, Feld MS (1997) Single molecule detection using surface-enhanced raman scattering (SERS). Phys Rev Lett 78:1667–1670
81. Blackie EJ, Le Ru EC, Meyer M, Etchehoin PG (2007) Surface enhanced raman scattering enhancement factors: a comprehensive study. J Phys Chem C 111:13794–13803
82. Nie S, Emory SR (1997) Probing single molecules and single nanoparticles by surface-enhanced Raman scattering. Science 275:1102–1106
83. Messinger BJ, Raben KUV, Chang RK, Barber PW (1981) Local fields at the surface of noble-metal microspheres. Phys Rev B 24:649–657
84. Wang DS, Kerker M (1981) Enhanced raman scattering by molecules adsorbed at the surface of colloidal spheroids. Phys Rev B 24:1777–1790
85. Fleischmann M, Hendra PJ, McQuillan AJ (1974) Raman spectra of pyridine adsorbed at a silver electrode. Chem Phys Lett 26:163–166
86. Moskovits M (2006) Surface-enhanced Raman spectroscopy: a brief perspective. In: Kneipp KM, Kneipp H (eds) Surface-enhanced Raman scattering – physics and applications. Springer, Berlin/New York, pp 1–18
87. Campion A, Kambhampati P (1998) Surface-enhanced raman scattering. Chem Soc Rev 27:241–250
88. Dousti MR, Sahar MR, Amjad RJ, Ghoshal SK, Awang A (2013) Surface enhanced raman scattering and up-conversion emission by silver nanoparticles in erbium–zinc–tellurite glass. J Lumin 143:368–373
89. Amjad RJ, Sahar MR, Dousti MR, Ghoshal SK, Jamaludin MNA (2013) Surface enhanced Raman scattering and plasmon enhanced fluorescence in zinc-tellurite glass. Opt Express 21:14282–14290
90. Som T, Karmakar B (2009) Nanosilver enhanced upconversion fluorescence of erbium ions in Er^{3+}: Ag-antimony glass nanocomposites. J Appl Phys 105:013102–013108
91. Amjad RJ, Sahar MR, Ghoshal SK, Dousti MR, Samavati AR, Riaz S, Tahir BA (2013) Spectroscopic investigation of rare-earth doped phosphate glasses containing silver nanoparticles. Acta Phys Pol A 123:746–749
92. Karmakar B, Som T, Singh SP, Nath M (2010) Nanometal-glass hybrid nanocomposites: synthesis, properties and applications. Trans Indian Ceram Soc 69:171–186
93. Speranza G, Minati L, Chiasera A, Ferrari M, Righini GC, Ischia G (2009) Quantum confinement and matrix effects in silver-exchanged soda lime glasses. J Phys Chem C 113:4445–4450
94. Kassab LR, De Araújo CB, Kobayashi RA, Pinto RDA, Silva DM (2007) Influence of silver nanoparticles in the luminescence efficiency of Pr^{3+} -doped tellurite glasses. J Appl Phys 102:103515
95. Som T, Karmakar B (2009) Enhancement of Er^{3+} upconverted luminescence in Er^{3+}: Au-antimony glass dichroic nanocomposites containing hexagonal Au nanoparticles. J Opt Soc Am B 26:B21–B27
96. Dousti MR, Sahar MR, Ghoshal SK, Amjad SK, Samavati AR (2013) Effect of AgCl on spectroscopic properties of erbium doped zinc tellurite glass. J Mol Struct 1035:6–12
97. Dousti MR, Ghassemi P, Sahar MR, Mahraz ZSA (2014) Chemical durability and thermal astability of Er^{3+}-doped zinc tellurite glass containing silver nanaparticles. Chalcogenide Lett 11:111–119
98. Silva AP, Carmo AP, Anjos V, Bell MJV, Kassab LRP, Pinto RDA (2011) Temperature coefficient of optical path of tellurite glasses doped with gold nanoparticles. Opt Mater (Amst) 34:239–243

99. Adamiv VT, Bolesta IM, Burak YV, Gamernyk RV, Karbovnyk ID, Kolych II, Kovalchuk MG, Kushnir OO, Periv MV, Teslyuk IM (2014) Nonlinear optical properties of silver nanoparticles prepared in Ag doped borate glasses. Phys B Condens Matter 449:31–35
100. Mai HH, Kaydashev VE, Tikhomirov VK, Janssens E, Shestakov MV, Meledina M, Turner S, Van Tendeloo G, Moshchalkov VV, Lievens P (2014) Nonlinear optical properties of Ag nanoclusters and nanoparticles dispersed in a glass host. J Phys Chem C 118:15995–16002
101. Ganeev RA, Ryasnyansky AI, Stepanov AL, Usmanov T (2004) Characterization of nonlinear optical parameters of copper- and silver-doped silica glasses at $\lambda = 1064$ nm. Phys Status Solidi 241:935–944
102. Som T, Karmakar B (2009) Core-shell Au-Ag nanoparticles in dielectric nanocomposites with plasmon-enhanced fluorescence: a new paradigm in antimony glasses. Nano Res 2:607–616
103. Wu Y, Xu T, Shen X, Dai S, Nie Q, Wang X, Song B, Zhang W, Lin C (2011) Effect of silver nanoparticles on spectroscopic properties of Er^{3+} -doped bismuth glass. In: Proceedings of the 6th IEEE Conference on Industrial Electronics and Applications, Beijing, China, pp 1464–1467
104. Dousti MR, Sahar MR, Amjad RJ, Ghoshal SK, Khorramnazari A, Dordizadeh Basirabad A, Samavati A (2012) Enhanced frequency upconversion in Er^{3+}-doped sodium lead tellurite glass containing silver nanoparticles. Eur Phys J D 66:237
105. Rao GV, Shashikala HD (2014) Optical, dielectric and mechanical properties of silver nanoparticle embedded calcium phosphate glass. J Non Cryst Solids 402:204–209
106. Dousti MR, Sahar MR, Ghoshal SK, Amjad RJ, Arifin R (2012) Up-conversion enhancement in Er^{3+}-Ag Co-doped zinc tellurite glass: effect of heat treatment. J Non Cryst Solids 358:2939–2942
107. Lin A, Son DH, Ahn IH, Song GH, Han W-T (2007) Visible to infrared photoluminescence from gold nanoparticles embedded in Germano-silicate glass fiber. Opt Express 15:6374–6379
108. Hayakawa T, Selvan ST, Nogami M (1999) Enhanced fluorescence from Eu^{3+} owing to surface plasma oscillation of silver particles in glass. J Non-Cryst Solids 259:16–22
109. Hayakawa T, Furuhashi K, Nogami M (2004) Enhancement of 5D0-7FJ emissions of Eu^{3+} ions in the vicinity of polymer-protected Au. J Phys Chem B 108:11301–11307
110. De Almeida R, da Silva DM, Kassab LRP, de Araujo CB (2008) Eu^{3+} luminescence in tellurite glasses with gold nanostructures. Opt Commun 281:108–112
111. Kassab LRP, da Silva DS, de Almeida R, de Araújo CB (2009) Photoluminescence enhancement by gold nanoparticles in Eu[sup $^{3+}$ doped GeO_2–Bi_2O_3 glasses. Appl Phys Lett 94:101912
112. Amjad RJ, Dousti MR, Sahar MR, Shaukat SF, Ghoshal SK, Sazali ES, Nawaz F (2014) Silver nanoparticles enhanced luminescence of Eu^{3+}-doped tellurite glass. J Lumin 154:316–321
113. Dousti MR, Sahar MR, Rohani MS, Samavati A, Mahraz ZSA, Amjad RJ, Awang A, Arifin R (2014) Nano-silver enhanced luminescence of Eu^{3+}-doped lead tellurite glass. J Mol Struct 1065–1066:39–42
114. Jiménez JA, Lysenko S, Liu H (2008) Enhanced UV-excited luminescence of europium ions in silver/tin-doped glass. J Lumin 128:831–833
115. Li L, Yang Y, Zhou D, Yang Z, Xu X, Qiu J (2013) Investigation of the interaction between different types of Ag species and europium ions in $Ag^{+} - Na^{+}$ ion-exchange glass. Opt Mater Express 3:806
116. Jiao Q, Qiu J, Zhou D, Xu X (2014) Contribution of Eu ions on the precipitation of silver nanoparticles in Ag-Eu Co-doped borate glasses. Mater Res Bull 51:315–319
117. Riano LP, de Araujo CB, Malta OL, Santa Cruz P, Couto dos Santos MA (2004) Growth of metallic Ag nanoparticles in fluoroborate glasses doped with rare-earth ions and their optical characterization. Proc SPIE 5622:551–555

118. Wei R, Li J, Gao J, Guo H (2012) Enhancement of Eu^{3+} luminescence by Ag species (Ag NPs, ML- Ag, Ag^{+}) in oxyfluoride glasses. J Am Ceram Soc 95:3380–3382
119. Kumar KVA, Revathy KP, Prathibha V, Sunil T, Biju PR, Unnikrishnan NV (2013) Structural and luminescence enhancement properties of Eu^{3+}/Ag nanocrystallites doped SiO_2-TiO_2 matrices. J Rare Earths 31:441–448
120. Culea E, Vida-Simiti I, Borodi G, Culea EN, Stefan R, Pascuta P (2014) Structural and spectroscopic effects of Ag–Eu^{3+} codoping of TeO_2–PbO glass ceramics. J Mater Sci 49:4620–4628
121. Buch Z, Kumar V, Mamgain H, Chawla S (2013) Silver nanoprism enhanced fluorescence in YVO4: Eu^{3+} nanoparticles. Chem Commun 49:9485–9487
122. Guo H, Wang X, Chen J, Li F (2010) Ultraviolet light induced white light emission in Ag and Eu^{3+} Co-doped oxyfluoride glasses. Opt Express 18:18900–18905
123. Strohhöfer C, Polman A (2002) Silver as a sensitizer for erbium. Appl Phys Lett 81:1414
124. Chiasera A, Ferrari M, Mattarelli M, Montagna M, Pelli S, Portales H, Zheng J, Righini GC (2005) Assessment of spectroscopic properties of erbium ions in a soda-lime silicate glass after silver–sodium exchange. Opt Mater 27:1743–1747
125. Portales H, Mattarelli M, Montagna M, Chiasera A, Ferraris M, Martucci A, Mazzoldi P, Pelli S, Righini GC (2005) Investigation of the role of silver on spectroscopic features of Er^{3+}-activated Ag-exchanged silicate and phosphate glass. J Non Cryst Solids 351:1738–1742
126. Fukushima M, Managaki N, Fujii M, Yanagi H, Hayashi S (2005) Enhancement of 1.54-Mm emission from Er-doped Sol–gel SiO2 films by Au nanoparticles doping. J Appl Phys 98:024316
127. Lin A, Boo S, Moon DS, Jeong HJ, Chung Y, Han W-T (2007) Luminescence enhancement by Au nanoparticles in Er^{3+}-doped Germano-silicate optical fiber. Opt Express 15:8603–8608
128. Watekar PR, Ju S, Han W-T (2008) Optical properties of the alumino-silicate glass doped with Er-ions/Au particles. Colloids Surf A Physicochem Eng Asp 313–314:492–496
129. Singh SK, Giri NK, Rai DK, Rai SB (2010) Enhanced upconversion emission in Er^{3+}-doped tellurite glass containing silver nanoparticles. Solid State Sci 12:1480–1483
130. Rivera VAG, Osorio SPA, Ledemi Y, Manzani D, Messaddeq Y, Nunes LAO, Marega E (2010) Localized surface plasmon resonance interaction with Er^{3+}-doped tellurite glass. Opt Express 18:25321–25328
131. Rivera VAG, Ledemi Y, Osorio SPA, Manzani D, Messaddeq Y, Nunes LAO, Marega E (2012) Efficient plasmonic coupling between Er^{3+}:(Ag/Au) in tellurite glasses. J Non Cryst Solids 358:399–405
132. De Campos VPP, Kassab LRP, de Assumpção TAA, da Silva DS, de Araújo CB (2012) Infrared-to-visible upconversion emission in Er^{3+} doped TeO_2-WO_3-Bi_2O_3 glasses with silver nanoparticles. J Appl Phys 112:063519
133. Amjad RJ, Sahar MR, Ghoshal SK, Dousti MR, Riaz S, Tahir BA (2012) Enhanced infrared to visible upconversion emission in Er^{3+} doped phosphate glass: role of silver nanoparticles. J Lumin 132:2714–2718
134. Amjad RJ, Sahar MR, Ghoshal SK, Dousti MR, Riaz S, Samavati AR, Jamaludin MNA, Naseem S (2013) Plasmon enhanced upconversion fluorescence in Er^{3+}: Ag phosphate glass: effect of heat treatment. Chin Phys Lett 30:027301
135. Amjad RJ, Sahar MR, Ghoshal SK, Dousti MR, Riaz S, Samavati AR, Arifin R, Naseem S (2013) Annealing time dependent up-conversion luminescence enhancement in magnesium–tellurite glass. J Lumin 136:145–149
136. Dousti MR, Sahar MR, Ghoshal SK, Amjad RJ, Arifin R (2013) Plasmonic enhanced luminescence in Er^{3+}: Ag Co-doped tellurite glass. J Mol Struct 1033:79–83
137. Qi Y, Zhou Y, Wu L, Yang F, Peng S, Zheng S, Yin D, Wang X (2014) Annealing time dependent 1.53 μm fluorescence enhancement in Er^{3+}-doped tellurite glasses containing silver NPs. Mater Lett 125:56–58

138. Culea E, Vida-Simiti I, Borodi G, Nicolae Culea E, Stefan R, Pascuta P (2014) Effects of Er^{3+}: Ag codoping on structural and spectroscopic properties of lead tellurite glass ceramics. Ceram Int 40:11001–11007
139. Awang A, Ghoshal SK, Sahar MR, Dousti MR, Amjad RJ, Nawaz F (2013) Enhanced spectroscopic properties and Judd–Ofelt parameters of Er-doped tellurite glass: effect of gold nanoparticles. Curr Appl Phys 13:1813–1818
140. Ghoshal SK, Awag A, Saar MR, Amjad RJ, Dousti MR (2013) Spectroscopic and structural properties of TeO_2-ZnO-Na_2O-Er_2O_3-Au glasses. Chalcogenide Lett 10:411–420
141. Sazali ES, Sahar MR, Ghoshal SK, Arifin R, Rohani MS, Awang A (2014) Optical properties of gold nanoparticle embedded Er^{3+} doped lead–tellurite glasses. J Alloys Compd 607:85–90
142. Awang A, Ghoshal SK, Sahar MR, Arifin R, Nawaz F (2014) Non-spherical gold nanoparticles mediated surface plasmon resonance in Er^{3+} doped zinc–sodium tellurite glasses: role of heat treatment. J Lumin 149:138–143
143. Awang A, Ghoshal SK, Sahar MR, Dousti MR, Nawaz F (2014) Growth of Au nanoparticles stimulate spectroscopic properties of Er^{3+} doped TeO_2-ZnO-Na_2O glasses. Adv Mater Res 895:254–259
144. Qi J, Xu T, Wu Y, Shen X, Dai S, Xu Y (2013) Ag nanoparticles enhanced near-IR emission from Er^{3+} ions doped glasses. Opt Mater 35:2502–2506
145. Mahraz ZSA, Sahar MR, Ghoshal SK, Dousti MR, Amjad RJ (2013) Silver nanoparticles enhanced luminescence of Er^{3+} ions in boro-tellurite glasses. Mater Lett 112:136–138
146. Obadina VO (2013) Investigation of silver nanostructures and their influence on the fluorescence spectrum of erbium-doped glasses. Opt Photonics J 03:45–50
147. Dousti MR, Amjad RJ, Mahraz ZAS (2014) Enhanced greena Nd red upconversion emissions in Er^{3+}doepd boro-tellurite glass containing gold nanoparticles. J Mol Struct 1079:347–352
148. Pan Z, Ueda A, Aga R, Burger A, Mu R, Morgan SH (2010) Spectroscopic studies of Er^{3+} doped Ge-Ga-S glass containing silver nanoparticles. J Non Cryst Solids 356:1097–1101
149. Speranza G, Bhaktha SNB, Chiappini A, Chiasera A, Ferrari M, Goyes C, Jestin Y, Mattarelli M, Minati L, Montagna M et al (2006) Nanocomposite Er–Ag silicate glasses. J Opt A Pure Appl Opt 8:S450–S454
150. Da Silva DM, Kassab LRP, Lüthi SR, de Araújo CB, Gomes ASL, Bell MJV (2007) Frequency upconversion in Er^{3+} doped PbO–GeO_2 glasses containing metallic nanoparticles. Appl Phys Lett 90:081913
151. Kassab LRP, Bomfim FA, Martinelli JR, Wetter NU, Neto JJ, Araújo CB (2009) Energy transfer and frequency upconversion in Yb^{3+}–Er^{3+}-doped PbO-GeO_2 glass containing silver nanoparticles. Appl Phys B 94:239–242
152. Qi Y, Zhou Y, Wu L, Yang F, Peng S, Zheng S, Yin D (2014) Silver nanoparticles enhanced 1.53 μm band fluorescence of Er^{3+}/Yb^{3+} codoped tellurite glasses. J Lumin 153:401–407
153. De Araujo CB, Silvério da Silva D, Alves de Assumpção TA, Kassab LRP, Mariano da Silva D (2013) Enhanced optical properties of germanate and tellurite glasses containing metal or semiconductor nanoparticles. Sci World J 2013:385193
154. Ma Y, Lin J, Chen J, Feng Z, Wei H, Mao J (2011) Plasmon-enhanced luminescence of YAG: Yb, Er nanopowders by Ag nanoparticles embedded in silicate glass. Mater Lett 65:282–284
155. Som T, Karmakar B (2011) Synthesis and enhanced photoluminescence in novel Aucore Au–Agshell nanoparticles embedded Nd^{3+}-doped antimony oxide glass hybrid nanocomposites. J Quant Spectrosc Radiat Transf 112:2469–2479
156. Da Silva DS, de Assumpção TAA, Kassab LRP, de Araújo CB (2014) Frequency upconversion in Nd^{3+} doped PbO–GeO2 glasses containing silver nanoparticles. J Alloys Compd 586:S516–S519
157. Dousti MR (2013) Efficient infrared-to-visible upconversion emission in Nd^{3+}-doped PbO-TeO_2 glass containing silver nanoparticles. J Appl Phys 114:113105
158. Som T, Karmakar B (2010) Surface plasmon resonance and enhanced fluorescence application of single-step synthesized elliptical nano gold-embedded antimony glass dichroic nanocomposites. Plasmonics 5:149–159

159. Som T, Karmakar B (2010) Enhanced frequency upconversion of Sm^{3+} ions by elliptical Au nanoparticles in dichroic Sm^{3+}: Au-antimony glass nanocomposites. Spectrochim Acta A Mol Biomol Spectrosc 75:640–646
160. Som T, Karmakar B (2009) Surface plasmon resonance in nano-gold antimony glass–ceramic dichroic nanocomposites: one-step synthesis and enhanced fluorescence application. Appl Surf Sci 255:9447–9452
161. Dousti MR (2014) Plasmonic effect of silver nanoparticles on the upconversion emissions of Sm^{3+}-doped sodium-borosilicate glass. Measurement 56:117–120
162. Li L, Yang Y, Zhou D, Yang Z, Xu X, Qiu J (2013) Investigation of the role of silver species on spectroscopic features of Sm^{3+}-activated sodium–aluminosilicate glasses via $Ag^{+} - Na^{+}$ ion exchange. J Appl Phys 113:193103
163. Jiménez JA, Sendova M (2012) In situ isothermal monitoring of the enhancement and quenching of Sm^{3+} photoluminescence in Ag Co-doped glass. Solid State Commun 152:1786–1790
164. Dyrba M, Miclea P-T, Schweizer S (2010) Surface plasmons for fluorescence enhancement in Sm-doped borate glasses. Radiat Meas 45:314–316
165. Fauzia Abdullah NA, Sahar MR, Hamzah K, Ghoshal SK (2014) Luminescence enhancement of samarium-doped tellurite glass containing silver nanoparticles. Adv Mater Res 895:260–264
166. Kaur G, Verma RK, Rai DK, Rai SB (2012) Plasmon-enhanced luminescence of Sm complex using silver nanoparticles in polyvinyl alcohol. J Lumin 132:1683–1687
167. Rai S, Bokatial L, Dihingia PJ (2011) Effect of CdS nanoparticles on fluorescence from Sm^{3+} doped SiO_2 glass. J Lumin 131:978–983
168. Jiménez JA (2013) Influence of Ag nanoparticles on the luminescence dynamics of Dy^{3+} ions in glass: the "plasmonic diluent" effect. Phys Chem Chem Phys 15:17587–17594
169. Dousti MR, Hosseinian SR (2014) Enhanced upconversion emission of Dy^{3+}-doped tellurite glass by heat-treated silver nanoparticles. J Lumin 154:218–223
170. Jiménez JA, Hockenbury JB (2013) Spectroscopic properties of CuO, SnO, and Dy_2O_3 Co-doped phosphate glass: from luminescent material to plasmonic nanocomposite. J Mater Sci 48:6921–6928
171. Petit L, Griffin J, Carlie N, Jubera V, García M, Hernández FE, Richardson K (2007) Luminescence properties of Eu^{3+} or Dy^{3+}/Au Co-doped SiO_2 nanoparticles. Mater Lett 61:2879–2882
172. De Assumpção TAA, da Silva DM, Camilo ME, Kassab LRP, Gomes ASL, de Araújo CB, Wetter NU (2012) Frequency upconversion properties of Tm^{3+} doped TeO_2–ZnO glasses containing silver nanoparticles. J Alloys Compd 536:S504–S506
173. Assumpção TAA, da Silva DM, Kassab LRP, de Araújo CB (2009) Frequency upconversion luminescence from Yb^{3+}–Tm^{3+} codoped PbO–GeO_2 glasses containing silver nanoparticles. J Appl Phys 106:063522
174. De Assumpção TAA, Da Silva DMM, Kassab LRP, Martinelli JRR, De Araújo CB (2010) Influence of the temperature on the nucleation of silver nanoparticles in Tm^{3+}/Yb^{3+} codoped PbO–GeO_2 glasses. J Non Cryst Solids 356:2465–2467
175. Kassab LRP, Freitas LF, Assumpção TAA, Silva DM, Araújo CB (2011) Frequency upconversion properties of Ag: TeO_2–ZnO nanocomposites codoped with Yb^{3+} and Tm^{3+} ions. Appl Phys B 104:1029–1034
176. Kassab LPR, Ferreira Freitas L, Ozga K, Brik MG, Wojciechowski A (2010) ZnO–TeO_2–Yb/Tm glasses with silver nanoparticles as laser operated quantum electronic devices. Opt Laser Technol 42:1340–1343
177. Assumpção TAA, Kassab LRP, Gomes ASL, Araújo CB, Wetter NU (2010) Influence of the heat treatment on the nucleation of silver nanoparticles in Tm^{3+} doped PbO-GeO_2 glasses. Appl Phys B 103:165–169

178. Qi J, Xu Y, Huang F, Chen L, Han Y, Xue B, Zhang S, Xu T, Dai S (2014) Photoluminescence of Ag nanoparticles and Tm^{3+} ions in the bismuth germanate glasses for the blue light-excited W-LED. J Am Ceram Soc 97:1471–1474
179. Camilo ME, Assumpção TAA, da Silva DM, da Silva DS, Kassab LRP, de Araújo CB (2013) Influence of silver nanoparticles on the infrared-to-visible frequency upconversion in Tm^{3+}/Er^{3+}/Yb^{3+} doped GeO_2-PbO glass. J Appl Phys 113:153507
180. Silva GH, Holgado DPA, Anjos V, Bell MJV, Kassab LRP, Amâncio CT, Moncorgè R (2014) Effect of Ag nanoparticles on the radiative properties of tellurite glasses doped with Er^{3+}, Yb^{3+} and Tm^{3+} ions. Opt Mater 2:6–11
181. Hu Y, Qiu J, Song Z, Yang Z, Yang Y, Zhou D, Jiao Q, Ma C (2014) Spectroscopic properties of Tm^{3+}/Er^{3+}/Yb^{3+} Co-doped oxyfluorogermanate glasses containing silver nanoparticles. J Lumin 145:512–517
182. Bi G, Wang L (2012) Photoluminescence enhancement induced from silver nanoparticles in Tb^{3+} -doped glass ceramics. Chin Opt Lett 10:092401
183. Piasecki P, Piasecki A, Pan Z, Ueda A, Aga R Jr, Mu R, Morgan SH (2010) Plasmon enhanced luminescence of Tb^{3+} doped Li_2O-LaF_3-Al_2O -SiO_2 glass containing Ag nanoparticles. Proc SPIE 7757:77572M
184. Piasecki P (2010) Formation of Ag nanoparticles and enhancement of Tb^{3+} luminescence in Tb and Ag Co-doped lithium-lanthanum-aluminosilicate glass. J Nanophotonics 4:043522
185. Li L, Yang Y, Zhou D, Xu X, Qiu J (2014) The influence of Ag species on spectroscopic features of Tb^{3+}-activated sodium–aluminosilicate glasses via $Ag+ - Na+$ ion exchange. J Non Cryst Solids 385:95–99
186. Zhang D, Hu X, Ji R, Zhan S, Gao J, Yan Z, Liu E, Fan J, Hou X (2012) Influence of Ag nanoparticles on luminescent performance of SiO2: Tb^{3+} nanomaterials. J Non Cryst Solids 358:2788–2792
187. Verma RK, Kumar K, Rai SB (2010) Pulsed laser ablation synthesis of silver nanoparticles and their use in fluorescence enhancement of Tb^{3+}-doped aluminosilicate glass. Solid State Commun 150:1947–1950
188. Kassab LRP, De Almeida R, da Silva DM, De Assumpão TAA, De Araújo CB, de Assumpção TAA, de Araújo CB (2009) Enhanced luminescence of Tb^{3+}/Eu^{3+} doped tellurium oxide glass containing silver nanostructures. J Appl Phys 105:103505
189. Pan Z, Sekar G, Akrobetu R, Mu R, Morgan SH (2011) Cooperative infrared to visible upconversion and visible to near-infrared quantum cutting in Tb and Yb Co-doped glass containing Ag nanoparticles. SPIE Proceedings 8096:809633–809633–7
190. Rai VK, Menezes LDS, de Araújo CB, Kassab LRP, Davinson M (2008) Surface-plasmon-enhanced frequency upconversion in Pr^{3+} doped tellurium-oxide glasses containing silver nanoparticles. J Appl Phys 103:093526
191. Naranjo LP, de Araújo CB, Malta OL, Cruz PAS, Kassab LRP (2005) Enhancement of Pr^{3+} luminescence in PbO–GeO_2 glasses containing silver nanoparticles. Appl Phys Lett 87:241914
192. Lakshminarayana G, Qiu J (2009) Enhancement of Pr^{3+} luminescence in TeO_2–ZnO–Nb_2O_5–MoO_3 glasses containing silver nanoparticles. J Alloys Compd 478:630–635
193. Qi Y, Zhou Y, Wu L, Yang F, Peng S, Zheng S, Yin D (2014) Enhanced upconversion emissions in Ho^{3+}/Yb^{3+} codoped tellurite glasses containing silver NPs. J Non Cryst Solids 402:21–27
194. Zhang WJ, Zhang QY, Chen QJ, Qian Q, Yang ZM, Qiu JR, Huang P, Wang YS (2009) Enhanced 2.0 microm emission and gain coefficient of transparent glass ceramic containing BaF_2: Ho^{3+}, Tm^{3+} nanocrystals. Opt Express 17:20952–20958